Diet-induced and mono-genetic obesity alter volatile organic compound signature in mice

Martin Kistler[1,2,5], Andreea Muntean[3], Wilfried Szymczak[3], Nadine Rink[4], Helmut Fuchs[1,2], Valerie Gailus-Durner[1,2], Wolfgang Wurst[6,7], Christoph Hoeschen[3], Martin Klingenspor[4], Martin Hrabě de Angelis[1,2,5,8], Jan Rozman[1,2,5,*]

[1]Institute of Experimental Genetics, Helmholtz Zentrum München, German Research Center for Environmental Health, Ingolstädter Landstrasse 1, 85764 Neuherberg, Munich, Germany

[2]German Mouse Clinic, Institute of Experimental Genetics, Helmholtz Zentrum München, German Research Center for Environmental Health, Ingolstädter Landstrasse 1, 85764 Neuherberg, Munich, Germany

[3]Research Unit Medical Radiation Physics and Diagnostics, Helmholtz Zentrum München, German Research Center for Environmental Health, Ingolstädter Landstrasse 1, 85764 Neuherberg, Munich, Germany

[4]ZIEL Department of Molecular Nutritional Medicine, Else Kröner-Fresenius Center, Technische Universität München, 85350 Freising, Germany

[5]German Center for Diabetes Research (DZD)

[6]Institute of Developmental Genetics, Helmholtz Zentrum München, German Research Center for Environmental Health, Ingolstädter Landstrasse 1, 85764 Neuherberg, Munich, Germany

[7]Developmental Genetics, Centre of Life and Food Sciences Weihenstephan, Technische Universität München, Freising, Germany

[8]Chair for Experimental Genetics, Life and Food Science Center Weihenstephan, Technische Universität Munich, D-85354 Freising-Weihenstephan, Germany

*Corresponding author. phone: +49 89 3187 3807; E-mail: jan.rozman@helmholtz-muenchen.de (J. Rozman), Postal: Institute of Experimental Genetics, Helmholtz Zentrum München, German Research Center for Environmental Health, Ingolstädter Landstrasse 1, 85764 Neuherberg, Munich, Germany

Abbreviations: VOCs, volatile organic compounds; HFD, high fat diet; LFD low fat diet; AUC, area under the curve; RF, random forest; ROC, receiver operating characteristic; FDR, false discovery rate; PTR-MS, proton transfer reaction mass spectrometry; TOF, time of flight; MC4R, melanocortin 4 receptor; MC4R-ki, MC4R W16X knock in; qNMR, quantitative nuclear magnetic resonance pk, peak; gt, genotype; adlib, ad libitum; MTMT, (methylthio)methanethiol; DMS, dimethyl sulfide; OGTT oral glucose tolerance test.

Character count: 48665

Abstract

Objective: The prevalence of obesity is still rising in many countries of the world and the multitude of consequential metabolic dysregulations such as type II diabetes mellitus that occur in patients exacerbate the impact on quality of life and public health systems. The analysis of volatile organic compounds (VOC) in breath that originate from multiple metabolic pathways provides an extraordinary potential to identify or monitor obese patients with increased risk profile for associated later diseases. In this study we aimed to describe the VOC patterns symptomatic for both general and model-specific obesity by analyzing samples of exhaled breath in diet-induced obese and mono-genetic obese mice.

Methods: We induced obesity by feeding a high fat diet to male C57BL/6J mice for 12 weeks (HFD). In addition, we analyzed male C57BL/6J mice carrying a global knock-in mutation in melanocortin-4 receptor (W16X, MC4R-ki). In both experimental groups, the source strengths of 208 volatile organic compounds were analyzed ad libitum fed and after overnight food restriction. Volatiles altered in obese mice were selected using the AUC-RF algorithm and tested using false discovery rate-controlled mixed effects model. A Gaussian graphical model was employed to identify chemical and metabolic links among the selected volatiles.

Results: In both models for obesity, volatiles relevant for the separation of obese and lean mice were detected (26 in MC4R-ki, 22 in HFD mice). Eight volatiles were found to be important in both obesity models. Interestingly, by creating a partial correlation network of the volatile metabolites, the chemical and metabolic origins of several volatiles were identified. HFD-induced obese mice showed an elevation in the ketone body acetone and acrolein, a marker of lipid peroxidation, and several unidentified volatiles. In MC4R-ki mice, several yet-unidentified VOCs were found to be altered. Remarkably, the pheromone (methylthio)methanethiol was found to be reduced, linking metabolic dysfunction and reproduction.

Conclusions: The signature of volatile metabolites can be instrumental to identify and monitor metabolic disease states, as shown in this screening of two obese mouse models. Our findings show the potential of breath gas analysis to non-invasively assess metabolic alterations for personalized diagnosis. Furthermore, breath gas analysis could aid in the stratification of patients with heterogeneous metabolic phenotypes and risk profiles.

Graphical abstract

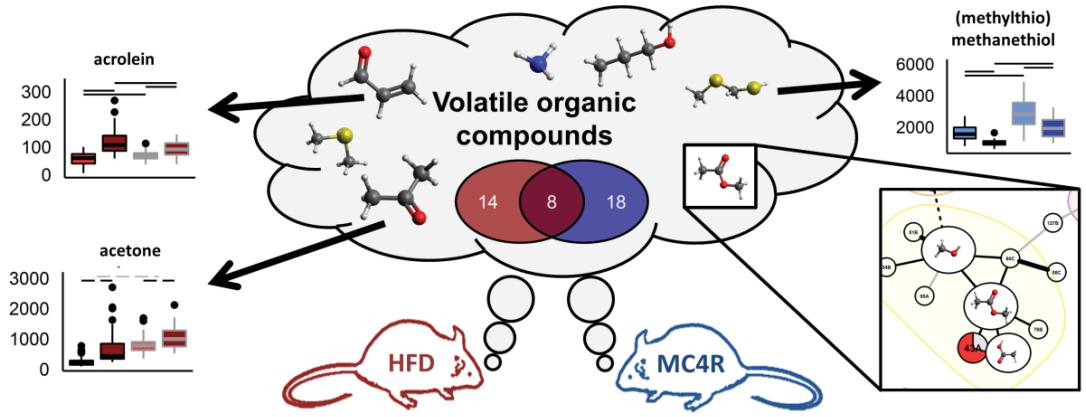

Keywords

High-fat diet; melanocortin 4 receptor; volatile organic compound; Gaussian graphical model; mouse pheromone; non-invasive metabolic phenotyping;

Highlights

- Both common and specific VOCs patterns emitted by HFD and MC4R mice
- HFD: Altered oxidative stress-associated and ketone body volatiles
- MC4R: MTMT reduction and a cluster altered likely consisting of (mono-)terpenes
- Gaussian graphical model is a valuable tool to detect VOC identity and pathways

1. Introduction

Obesity has progressed to a world-wide epidemic linked to a number of co-morbidities such as diabetes, cardiovascular disease, dyslipidemia and certain types of cancers (Guh *et al*, 2009). Easily accessible biomarkers are central for the assessment of individual risks of patients to suffer from such pathologies and to develop personalized medicine approaches for prevention and treatment. The dysregulation of metabolic pathways and the associated changes in body fluid metabolite concentrations are increasingly studied and also used for risk prediction (Mahendran *et al*, 2013; Elliott *et al*, 2015; Wahl *et al*, 2015). A variety of normal and disease-associated metabolic reactions produce small volatile organic compounds (VOCs) which can be detected in body fluids but also non-invasively in exhaled breath. Over the past decade, advances in the methodology made it possible to determine VOCs online in a concentration range of ppm to ppt and led to studies linking VOC signatures to various pathologies (Boots *et al*, 2012). Regarding diseases associated with energy metabolism, several human studies were conducted trying to monitor glucose levels (Lee *et al*, 2009; Minh *et al*, 2011), identify gestational, type1, or type 2 diabetes (Halbritter *et al*, 2012; Novak *et al*, 2007; Greiter *et al*, 2010), and characterize non-alcoholic fatty liver disease and liver cirrhosis (Morisco *et al*, 2013; Alkhouri *et al*, 2014). Prerequisites for broader clinical application are (I) clear identification of the molecules that are exhaled as VOCs and (II) a better understanding of the considerable inter- and intra-individual variation in VOCs found in breath even in healthy humans (Phillips *et al*, 1999; Basanta *et al*, 2012; Martinez-Lozano Sinues *et al*, 2014). Environmental "wash-in", the diet and associated microbial changes as well as circadian rhythm might increase this variation. Animal models, and especially rodent models, for human diseases are a tremendously valuable tool to deepen the understanding of molecular mechanisms and decipher the various sources of volatiles in a controlled environment (Rosenthal & Brown, 2007). In this study, we were particularly interested in differences in VOC signatures of normal weight mice and mice with manifested obesity induced either by feeding a high fat diet (HFD) or induced by targeted loss of function mutation of the melanocortin 4 receptor (Bolze *et al*, 2011). VOC signatures could reflect the degree of obesity but could also be due to changes in diet composition which is a confounding interaction that cannot be avoided in diet induced obesity studies (Baranska *et al*, 2013; Kistler *et al*, 2014). In contrast to diet-induced modifications of VOC signatures, to our knowledge no investigation on the effects of genetically-induced obesity on the volatilome, defined as the total amount of all VOCs emitted, was conducted so far. Therefore, the aim of this study was to characterize alterations in exhaled volatile organic compounds both in a diet-induced and a mono-genetic obese mouse model and to evaluate whether a symptomatic pattern of VOCs related to

obesity can be determined. In addition, individual changes in the volatilome of two specific obese models with distinct metabolic deregulations are of interest. We employed statistical analysis methods that identified typical correlations between VOC emission rates, in the following called source strengths that could be used to unravel the biochemical origin of the respective molecules.

2. Material and Methods

2.1. Mice, animal housing and challenge experiments

Mice were housed in in type IIL polycarbonate cages in individually ventilated cages (Tecniplast, Italy). A 12:12h light/dark cycle at a temperature of 24 ± 1 degree Celsius and air humidity of 50 – 60% were maintained. Animals were housed in groups of 2 to five animals per cage in specific pathogen-free conditions in the German Mouse Clinic (GMC) (Fuchs *et al*, 2009). Wood shavings were used for bedding (Altromin GmbH, Germany). For the generation of the diet-induced obesity model, 20 male C57BL/6J mice from in-house breeding were fed a pelleted laboratory chow from weaning on with a*d libitum* access to food and drinking water (no. 1314, Altromin, Lage, Germany). From the age of twelve weeks until the start of the VOC measurement (24± 2 weeks), the diet was changed to pelleted purified low fat and high fat diets (low fat: E 15000-04; high fat: E 15741-34; both: Ssniff, Soest, Germany). Assignment to diet groups was performed randomly using existing cage stocking to avoid single housing while ensuring balanced group numbers. A mono-genetic hyperphagic obesity model having a melanocortin-4-receptor nonsense allele W16X was used (Mc4r-ki mouse, as previously published (Bolze *et al*, 2011)). 15 homozygous MC4R-ki BL6/J mice as well as 15 controls were transferred to the GMC from the provider's lab at the age of 5 weeks and analyzed at the age of 24± 2 weeks. Mice had ad libitum access to drinking water and a pelleted laboratory chow from weaning on (<5 weeks: "RM-Z autoklavierbar", ssniff; >5 weeks: no. 1314, Altromin, Lage, Germany). All experiments were performed following animal welfare regulations with permission from the district government of Upper Bavaria (Regierung von Oberbayern).

For the analysis of VOCs from *ad libitum* fed mice*,* gas measurements took place between 1 pm and 6 pm. During this time, food consumption is low compared to nighttime. Therefore, this period was chosen to reduce contribution of food-derived volatiles to measured VOC patterns. Mice were measured in random order and alternating between control and obese mice to remove potential systemic bias. For the fasted VOC measurements, mice were food deprived overnight beginning

around 5-6 pm and were measured in the same order as in ad libitum state between 8 to 12 am the following day. Mice were weighed before every VOC measurement to the nearest 0.1 g and body composition was monitored by non-invasive qNMR scans in ad libitum fed state (Bruker Minispec LF50 body composition analyser, Ettlingen, Germany). The comparisons of body, lean and fat mass between groups were performed using a linear regression model.

2.2. Proton-transfer reaction time-of-flight mass spectrometry and protocol for real-time breath gas analysis in unrestrained mice

A high-sensitivity Proton Transfer Reaction Mass Spectrometer (PTR-MS, e.g. benzene 100 cps/pppV; PTR-MS, Ionicon Analytic GmbH, Innsbruck, Austria) with a resolution of Δm/m <= 2000 was used. The principle of PTR mass spectrometry using H_3O^+ ions to softly ionize and detect VOCs was developed in the late 1990s (Lindinger *et al*, 1998; Petersson *et al*, 2009). A drift tube temperature of 80 degrees Celsius, a drift tube voltage of 600 V and a drift pressure 2.3 mbar were applied. A mass range from m/z 0 to 349.5 was recorded (repetition rate of 77 kHz); the sum spectra with integration time of 3 s were stored (TOF-DAQ, Tofwerk AG, Switzerland). For the integration of peaks from the TOF-spectra the software PTR-MS Viewer was used (Version 3.2.6, Ionicon analytic GmbH, Innsbruck, Austria). An internal calibration with the known peaks $H_3{}^{18}O^+$ (m/z 21.0221), NO^+ (m/z 29.9971) and protonated acetone (m/z 59.0491, $C_3H_6O.H^+$) was performed. 306 peaks were selected manually from the spectra. The deconvolution of overlapping peaks was performed fitting a gaussian distribution to the peaks in the PTR-MS Viewer. VOC concentrations were calculated using a constant k-rate of $2 * 10^{-9}$ [$cm^3 * s^{-1}$] in the semi-quantitative estimation formula (Lindinger *et al*, 1998). The system sensitivity was controlled using a gas calibration unit (GCU, Ionicon Analytic GmbH, Innsbruck, Austria) with a mixture of substances (VOC gas standard, Ionicon Analytic GmbH, Innsbruck, Austria) regularly. From a set of compounds, a linear calibration curve obtained from multiple concentrations was used to calculate the individual transmission factors.

A setup and protocol for real-time measurement of breath gas analysis in unrestrained mice was used as described previously (Szymczak *et al*, 2014; Kistler *et al*, 2014). In brief, mice were acclimatized to a training respiratory chamber for 7 minutes. A measurement chamber connected to the mass spectrometer is flushed 2 minutes with a flow rate 3 l/min to dilute enclosed laboratory room air. After flushing, the VOCs from the empty respiratory chamber are measured as a blank (5 min, flow 60 mL min-1) to the detect system leakage and background VOCs. Signals monitored for leakage from laboratory air are acetone (m/z = 59.05) and propanol (m/z = 41.06) concentration.

Following this blank measurement, the system is switched to flushing state and the mouse is placed into the chamber. After the 2 min flushing, measurement phases alternate with flushing of the chamber, allowing the volatiles to accumulate in the gaseous phase.

During accumulation of VOCs in the headspace of unrestrained and non-anaesthetized mice, contaminations arise e.g. from urination and defecation. The measurement chamber was monitored for signs of contamination repeatedly during measurements. In addition, several volatiles were used as marker substances for urine or feces. Urine was detected online due to sudden changes in humidity (determined as water-cluster $(H_2{}^{18}O)_2.H^+$, m/z = 39.05), concentration of trimethylamine (m/z = 60.07) and pk127B (tentatively dimethyl trisulfide, m/z = 127.02). Concentration of methanethiol (m/z = 49.02) indicated presence of feces. In case of feces contamination, feces were removed and accumulation phase was skipped. If urine was present, the respirometry chamber was replaced, the mouse was gently cleaned using soft tissue paper (Kimtech Science, Kimberly-Clark) and the measurement was restarted.

2.3. Data analysis and statistics

2.3.1. Calculation of source strength and data pre-procession

Measurement start and end were defined manually using an in-house web-application based on R and shiny package (R Core Team (2014); Chang *et al*, 2015). A compartment model was used to describe the emission of a certain peak from recorded saturation curves (non-linear regression, described in (Szymczak *et al*, 2014)). This model resulted in a source strength [ppb*ml/min], which we used for further analyses. The information of group membership was not recorded in raw data files but added later on to ensure fully blinded analysis of saturation curves. As further contamination control step, data was filtered for high concentrations or sudden increases of urinary and feces markers (pk127B, pk60 and pk49 > 1 ppb). The individual source strengths (1-5 per mouse and feeding state) were differentially corrected against the respective blank source strength of an empty box to account for possible micro-leakage or background system emission. For every peak, outliers (defined as greater 5 standard deviations from mean) were removed. Peak data and single measurement data with more than 10% missing values were excluded. Peaks with source strengths not different or lower compared to corresponding blank source strengths were excluded as well (linear regression modelling with $p < 0.1$ to ensure enclosure of low signal candidate VOCs). An

exception was made for known oxygen isotopes, as the negative source strength (=consumption) is expected. This filter steps resulted in a final group sizes of 15 for fasted MC4R-wt mice, 14 for fasted MC4R-ki mice, 11 for ad libitum fed MC4R-wt mice and 9 for every other experimental group. As a complete data-matrix is required to calculate random forest and gaussian graphical models, missing data was imputed using chained equations (mice R package (van Buuren & Groothuis-Oudshoorn, 2011)), which accounted for 0.29% of data.

2.3.2. **Feature selection and statistical testing of individual VOCs**

Using a time-of-flight mass spectrometric detection of volatiles, the dataset consisted of a large number of peaks relative to animal numbers. We applied the AUC-RF (Area under the curve – random forest) algorithm as recently published (Urrea & Calle, 2012) to find a reduced set of candidate volatiles. In this algorithm, an initial random forest is computed to obtain a ranking of predictors and an area-under-the receiver operating characteristic (ROC) curve. During the elimination process, less important variables are removed and AUCs of the resulting RFs are computed; an optimal set of predictors based on the AUC is finally reported. We used this algorithm for both HFD-fed and MC4R-ki datasets independently; setting strata to allow only one measurement per mouse and fasting status in every decision tree. A five-fold cross validation was applied 20 times to avoid over-fitting of each of the resulting RF model (using again a modified version of the algorithm allowing for stratification). Peaks with a selection probability higher than 70% in the cross-validation AUC-RFs were used for further analysis.

For the analysis of genotype-induced and diet-induced effects on the VOC source strengths, two-sided mixed effects models were applied (Pinheiro *et al*, 2015). Both diet and genotype subsets of data were log-transformed to approximate a normal distribution (tested visually by qq-plotting). The variance between groups was controlled using both boxplots of source strength as well as residuals and residual versus fitted data plots. For every peak of both subsets of data, effects of the corresponding intervention variable (diet respectively genotype), the fasting status as well as the interaction of both were tested using a mixed effects model accounting for repeated measures. If a significant interaction could be detected, individual group comparisons were performed using multcomp r package (Hothorn *et al*, 2014). As a larger number of tests leads to summation of Type I – Error, control of false discovery rate after Benjamini and Hochberg (Benjamini & Hochberg, 1995) was applied and all p-values were adjusted according to a 10% FDR.

2.3.3. Data visualization and VOC identification using Gaussian graphical modelling

2.3.3.1. Heatmaps and boxplots

Both sets of data were visualized in a clustered heatmap using the Heatplus (Ploner, 2014) package from Bioconductor (Gentleman *et al*, 2004). Mean ad libitum fed as well as mean fasted source strength data per mouse was used and shown individually. Boxplots were created using the R package ggplot2 using all repeatedly measured source strength data (Wickham, 2009).

2.3.3.2. Gaussian graphical model

We applied a gaussian graphical model to log-transformed source strengths of breath volatiles to visualize information about fragmentation, isotopic, water cluster and/or metabolic correlations. The complete dataset features more variables than number of mice, therefore we used a shrinkage approach to estimate a partial correlation matrix (Schäfer & Strimmer, 2005). As the data is of longitudinal structure, we created a network accounting for that using dynamic (partial) correlation (Opgen-Rhein & Strimmer, 2006). A network was extracted from the estimated partial correlation matrix using a local false discovery rate of 3% (GeneNet R package (Schaefer *et al*, 2015). A "dummy" variable to correct for inter-experimental differences between HFD fed and MC4R-ki mice was included in the network but not plotted. For every peak within a selected subset with significant fasting state, genotype or diet effect, the percentaged coefficients from mixed effects model are shown in the nodes as a pie-chart. Top 20% of connections are shown with bold lines; minor 20% with grey lines, negative partial correlations with dotted lines. Direct positive connections of significant nodes were highlighted and combined for overlapping subnetworks containing multiple significant nodes. Peaks included in AUC-RF model data-subsets but without significant connections were included in the graphical model for illustration purposes.

2.3.4. Data availability

Data is accessible as a supplementary document.

3. Results

3.1. Obesity state of high-fat diet fed and mono-genetic mice

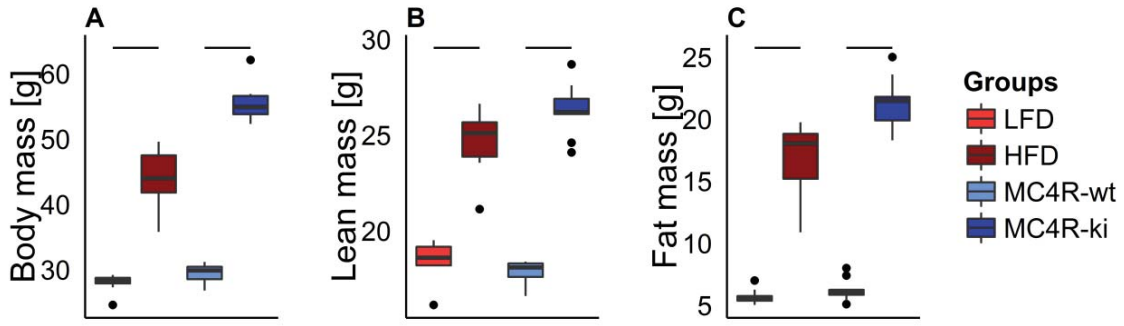

Figure 1: Body mass, lean mass and fat mass. Body mass (A), lean mass (B) and fat mass (C) for High Fat Diet fed (HFD, dark red) and melanocortin-4-receptor W16X knock-in (MC4R-ki, dark blue) mice as well as corresponding controls (Low-fat diet LFD, red; melanocortin-4-receptor wild type, MC4R-wt, blue) is shown in boxplots. Significant differences between controls and respective obesity mouse models are shown as black lines over individual boxes (linear regression model, $p<0.05$). Group sizes: MC4R-wt ad lib (n=11), other groups (n=9).

Both HFD and the MC4R-ki mutation resulted in clear states of obesity as was evident from increased body mass as well as lean and fat mass. HFD fed mice were heavier compared to littermate controls (44.21 ± 4.17 g vs 27.94 ± 1.47 g, $p=4.01*10^{-8}$, Fig. 1A). This gain in mass was partly due to an increase in lean mass (24.64 ± 1.7 g vs 18.47 ± 1.08 g, $p=2.56*10^{-7}$, Fig. 1 B) as well as an increase in fat mass (16.83 ± 2.88 g vs 5.69 ± 0.65 g, $p=2.16*10^{-8}$, Fig. 1C). For MC4R-ki mice, also a considerable difference in body mass compared to littermate controls could be detected (50.99 ± 3.19 g vs 28.01 ± 1.28 g, $p=2.00*10^{-14}$, Fig. 1 A). This difference was in part attributed to lean mass (26.28 ± 1.4 g vs 17.8 ± 0.64 g, $p=5.67*10^{-13}$, Fig. 1 B), but largely due to elevated fat mass (21.3 ± 2.09 g vs 6.2 ± 0.83 g, $p=1.77*10^{-14}$, Fig. 1 C). Overall, the impact of the MC4R-ki on body mass and body composition was more pronounced compared to the HFD model.

3.2. Selection of VOCs relevant for classification

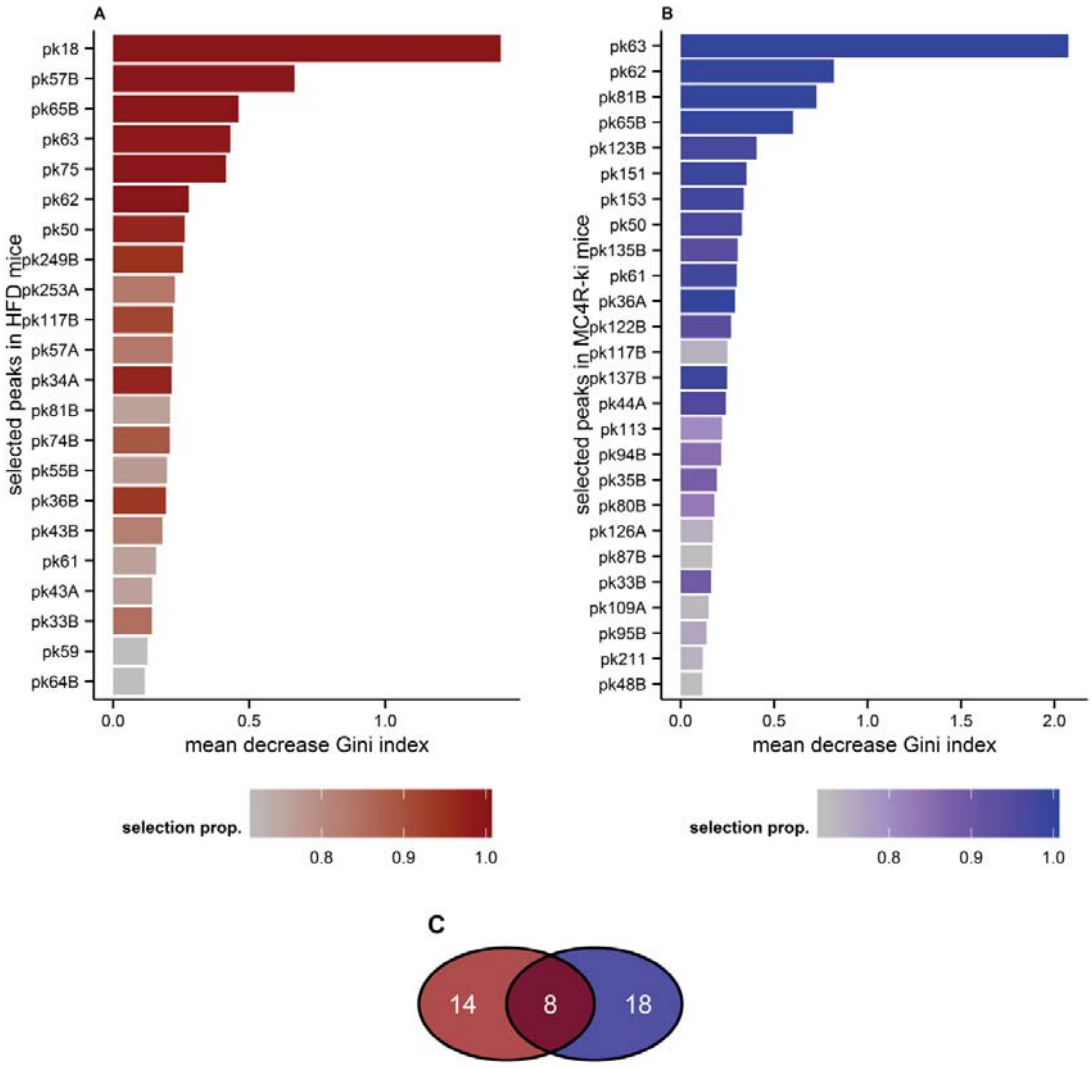

296

297 **Figure 2: Variable importance for peaks selected for alterations in obesity models.** Variable importance recursive feature
298 selection using AUC-OOB of random forest models in high fat diet fed mice (HFD, A) and melanocortin-4-receptor W16X
299 knock-in (MC4R-ki, B). Color gradients indicate selection probability after 20 iterations of a five-fold cross validation
300 procedure. Peaks with more than 70% selection probability are shown here and were selected for further analysis.
301 Overlapping of selected peaks is shown as Venn diagram (C).

302

303 For both obesity models, a feature selection was performed to classify obesity biomarkers by
304 optimization of the ROC area under the curve in a series of random forest models. A cutoff of at least
305 70% selection probability was used to select 22 candidate peaks with the highest variable
306 importance in HFD mice (Fig. 2A). For MC4R-ki mice, 26 candidate peaks fulfilled the cutoff criterion
307 (Fig. 2B). Interestingly, within these peaks with the highest classification importance an overlap of 8

peaks could be detected between the two mouse models (Fig. 2C). The eight peaks present in both groups were pk33B (methanol), pk50 (unassigned), pk61 (acetic acid), pk62 (MTMT), pk63 (CO_2, DMS), pk65B (CO_2, DMS isotopes), pk81B (unassigned) and pk117B (unassigned).

3.3. Visualization of selected source strength data

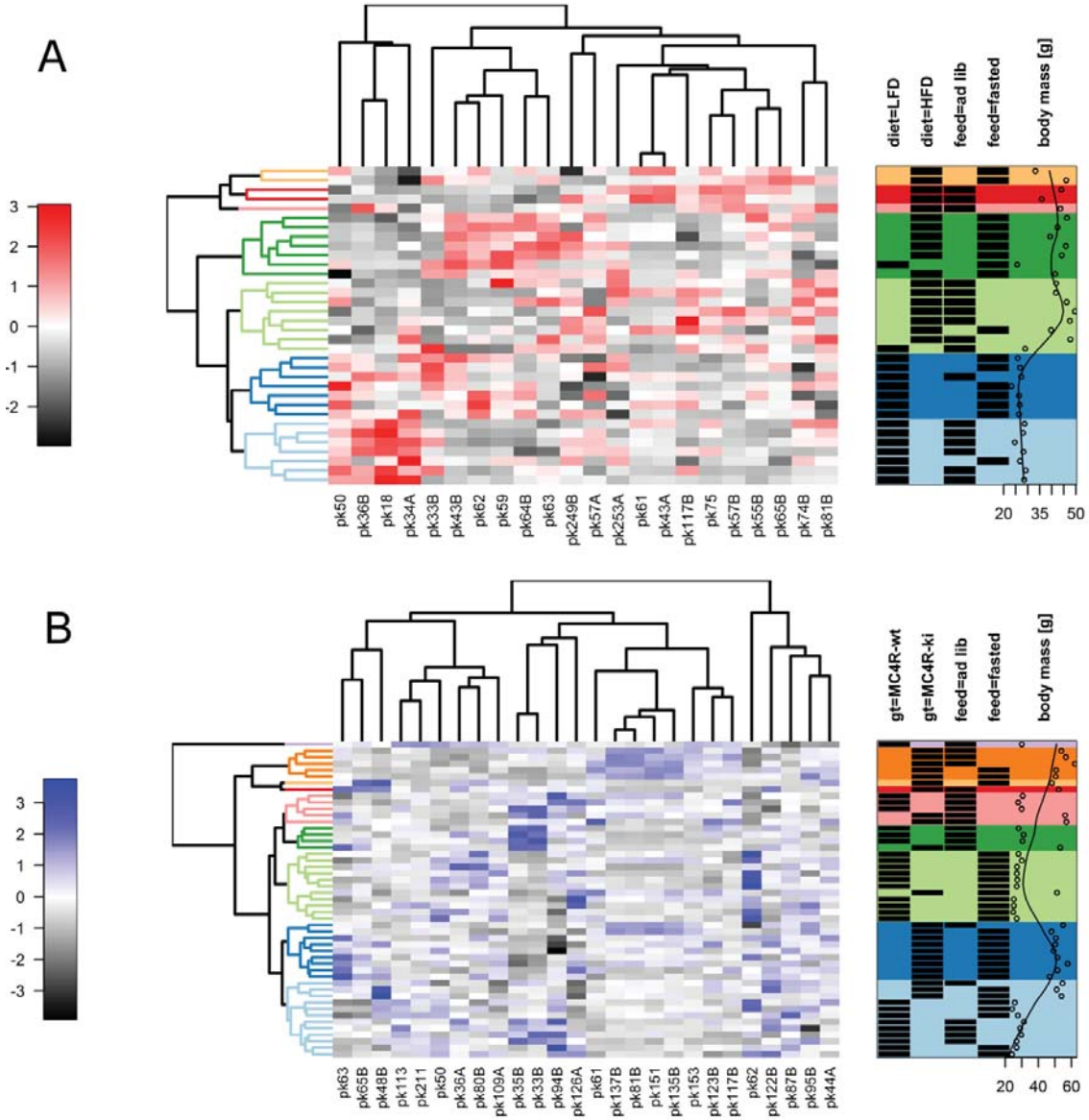

Figure 3: Heatmaps of selected VOCs. Heatmap of selected peaks in HFD fed (A) and MC4R-ki mice (B) are shown with hierarchical clustering of individual mice (mean data, rows, sub-clusters colored) and VOC peaks (columns, labels according to nominal mass). Data is scaled and centered. Color-coding legend shown on the left. Classification of individual mice is

annotated on the right (A: diet = LFD or HFD; B: gt = MC4R-wt or MC4R-ki; both feed = ad libitum fed or fasted, body mass [g], subcluster-membership colored). Group sizes: MC4R-ki fasted (n=15), MC4R-wt fasted (n=14), MC4R-wt ad lib (n=11), other groups (n=9).

Heatmaps consisting of RF-selected peaks for both models were created to get further insight into data structure by using unsupervised hierarchical clustering (Fig. 3). HFD fed mice clustered in the top half of the heatmap with a remote subgroup within the dark blue sub cluster (Fig. 3A). Interestingly, despite the selection for obesity relevant peaks, a clustering according to fasting status was observed (fasted within light red, light green and dark blue, predominantly). Contrary to the findings in HFD fed mice, the feeding status seemed to be the dominant clustering principle with MC4R wild type and knock-in mice showing fasted mice in the light green, dark blue and light blue sub clusters (Fig. 3B). Notably, fasted MC4R-ki mice clustered together mostly in the dark blue subcluster, whereas ad libitum fed knock-in mice showed a weaker clustering in the “warm colored” sub clusters.

3.4. Effects on VOC signature in diet-induced and monogenetic obesity

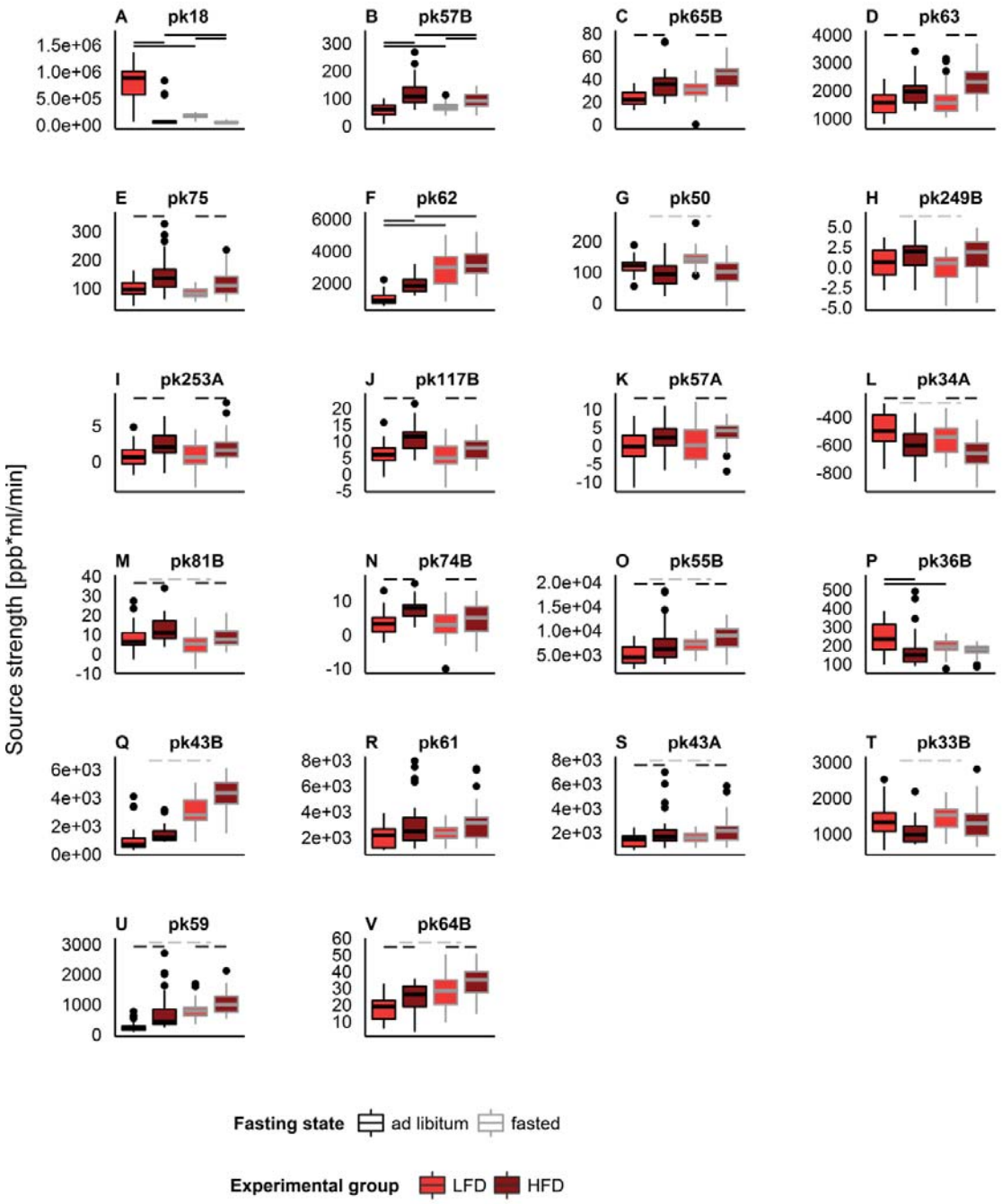

Figure 4: VOC source strengths affected by high fat diet or fasting. Source strengths for nominal mass-labelled peaks 18 (A), 57B (B), 65B (C), 63 (D), 75 (E), 62 (F),50 (G), 249B (H), 253A (I), 117B (J), 57A (K), 34A (L), 81B (M), 74B (N), 55B (O), 36B (P), 43B (Q), 61 (R), 43A (S), 33B (T), 59 (U) and 64B (V) are shown as boxplots (ordered after selection probability in cross-validated AUC-RF algorithm). Box fill corresponds to diet (red: low fat diet; dark red: high fat diet). Box border corresponds to fasting state (black: ad libitum fed; grey: fasted). Significant main effects in mixed effects model are shown as dotted

lines (black: diet, grey: fasting state). In case of interaction, significant group differences are shown as black lines. P-values are adjusted for a false discovery rate of 10 %. Group sizes (n=9).

In HFD mice several VOC source strengths were affected as shown by linear mixed effects modelling for diet and fasting effects (Fig. 4, Supplementary table 1). A significant increase in source strength could be found in eleven peaks. Those peaks are 65B (unassigned, Fig. 4 C), 63 (CO_2*H_2O/ DMS, Fig. 4 D), 75 (methyl acetate, Fig. 4 E), 253A (unassigned, Fig. 4 I), 117B (unassigned, Fig. 4 J), 57A (unassigned, Fig. 4 K), 81B (unassigned, Fig. 4 M), 74B (unassigned, Fig. 4 N), 55B (H_3O^+.H_2O/ C_4H_6.H^+, Fig. 4 O), 43A (C_2H_2O.H+, Fig. 4 S), 59 (acetone, Fig. 4 U) and 64B ($^{13}CO_2$.H_3O^+/ $^{13}CCH_6S$.H^+, Fig. 4 V). Source strength in peak 34A ($^{16}O^{18}O$, Fig.4 L) was decreased in diet-induced obese mice.

In the HFD model, several volatiles were affected by the fasting status of the mouse. Fasting induced higher emitted source strength in the seven peaks: 50 (unassigned, Fig. 4 G), 55B (H_3O^+.H_2O/ C_4H_6.H^+, Fig. 4 O), 43B (C_3H_6.H^+, Fig. 4 Q), 43A (C_2H_2O.H+, Fig. 4 S), 33B (methanol, Fig. 4 T), 59 (acetone, Fig. 4 U) and 64B ($^{13}CO_2$.H_3O^+/ $^{13}CCH_6S$.H^+, fig. 4 V). Three volatiles were reduced after overnight food restriction: 249B (unassigned, Fig. 4 H), 34A ($^{17}O_2$, Fig.4 L) and 81B (unassigned, Fig. 4 M).

In four peaks, an interaction of HFD feeding and food restriction was present. Ammonia (Fig. 4A, pk18) was decreased in HFD mice (with a larger decrease in source strengths in the ad libitum fed state) and upon overnight fasting. Acrolein (Fig 4B, pk57B (2-propenal, C_3H_4O.H^+)) was elevated in obese mice in both states. Upon fasting source strength was increased in wild type mice but decreased in HFD fed animals. Peak 62 was assigned to a thiol-loss fragment of (Methylthio)methanethiol (MTMT, CH_3SCH_2.H^+) as described in (Da Yu Lin *et al*, 2005) (Fig. 4F). MTMT was increased upon fasting in both groups. Furthermore, ad libitum fed HFD mice showed higher source strength of MTMT compared to LFD fed mice, an effect which was no longer present when fasted mice were measured in the morning. pk36B was decreased in HFD ad libitum fed mice and fasted LFD fed mice (Fig 4P, unassigned).

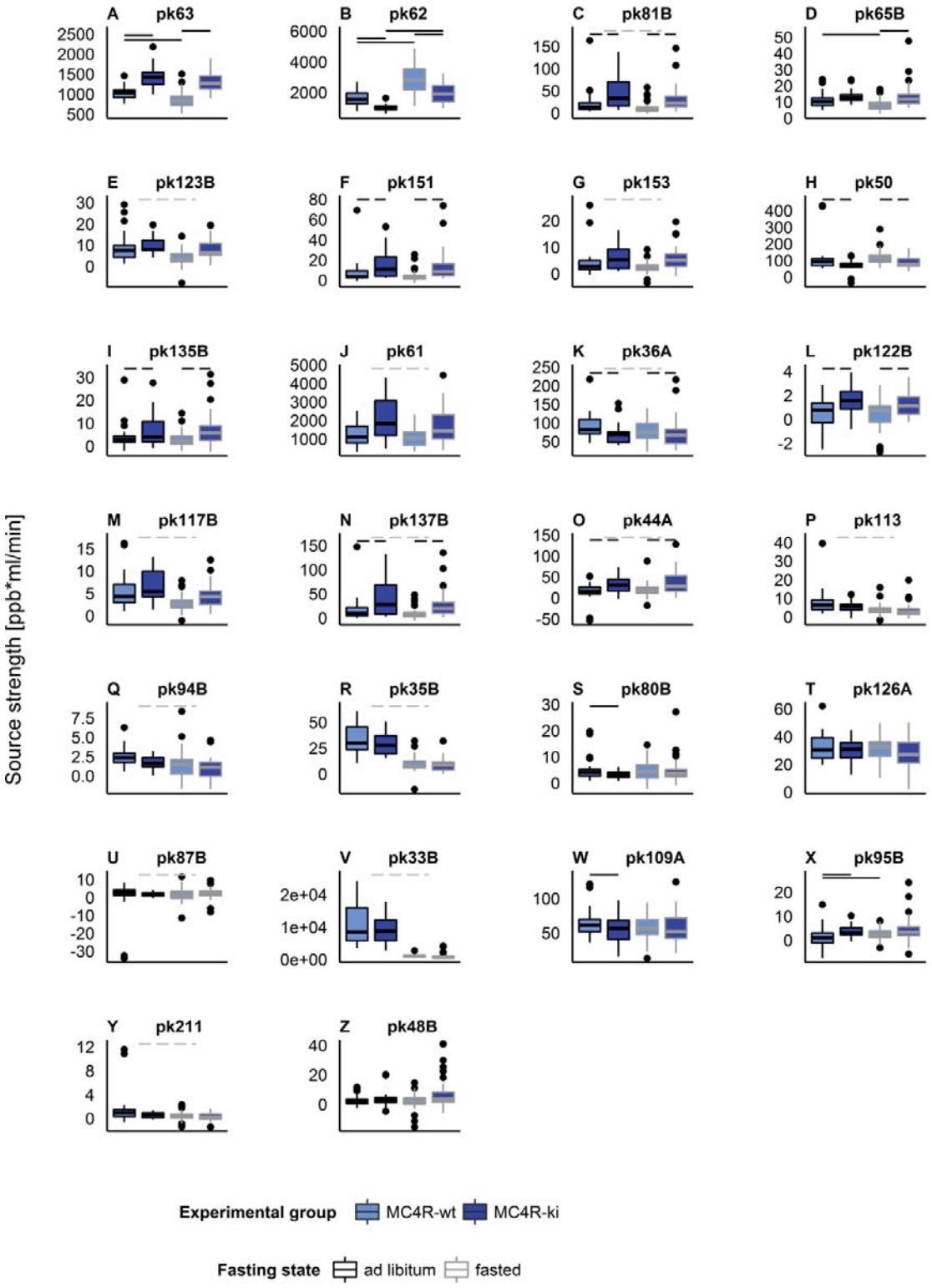

Figure 5: VOC source strengths affected by genotype or fasting. Source strengths for nominal mass-labelled peaks 63 (A), 62 (B), 81B (C), 65B (D), 123B (E), 151 (F), 153 (G), 50 (H), 135B (I), 61 (J), 36A (K), 122B (L), 117B (M), 137B (N), 44A (O), 113(P), 94B (Q), 35B (R), 80B (S), 126A (T), 87B (U), 33B (V), 109A (W), 95B (X), 211 (Y) and 48B (Z) shown as boxplots

(ordered after selection probability in AUC-RF feature selection). Box fill corresponds to genotype (blue: melanocortin-4-receptor wild type; dark blue: melanocortin-4-receptor W16X knock-in). Box border corresponds to fasting state (black: ad libitum fed; grey: fasted). Significant main effects in mixed effects model are shown as dotted lines (black: genotype, grey: fasting state). In case of interaction, significant group differences are shown as black lines. P-values are adjusted for a false discovery rate of 10 %. Group sizes: MC4R-ki fasted (n=15), MC4R-wt fasted (n=14), MC4R-wt ad lib (n=11), MC4R-ki ad lib (n=9).

In MC4R-ki mice several VOC source strengths differed between genotypes as shown by linear mixed effects modelling (Fig. 5, detailed model results in Supplementary table 1)**.** A significant increase was found in eight volatiles: peak 63 (CO2*H2O/ DMS, Fig. 5 A), 81B (unassigned, Fig. 5 C), 151 (unassigned, Fig. 5 F), 135B (unassigned, Fig. 5 I), 122B (unassigned, Fig. 5 L), 137B (unassigned, Fig. 5 N), 44A (C_2H_3O / $^{13}CCH_2O.H^+$, Fig. 5 O) and 95B (unassigned, Fig. 5 X). In five volatiles, a decrease in source strength was observed in MC4R-ki mice: peak 62 (MTMT, Fig. 5 B), 50 (unassigned, Fig. 5 H), 36A (unassigned, Fig 5 K), 80B (unassigned, Fig. 5 S) and 109A (unassigned, Fig. 5 W).

In addition to genotype effects, overnight food restriction affected four peaks positively and eleven peaks negatively. An increase in fasted state was observed in peaks 62 (MTMT, Fig. 5 B), 44A (C_2H_3O / $^{13}CCH_2O.H^+$, Fig. 5 O), 87B (unassigned, Fig. 5 U) and 95B (unassigned, Fig. 5 X). Decreased fasting source strengths were found for peaks 63 (CO_2*H_2O/ DMS, Fig. 5 A), 81B (unassigned, Fig. 5 C), 123B (unassigned, Fig. 5 E), 61 (acetic acid, Fig. 5 J), 36A (unassigned, Fig. 5 K), 117B (unassigned, Fig. 5 M), 137B (unassigned, Fig. 5 N), 113 (unassigned, Fig. 5 P), 94B (unassigned, Fig. 5 Q), 35B ($CH_3{}^{16}OH.H+$, Fig. 5 R) and 211 (unassigned, Fig. 5 Y).

An interaction of MC4R-ki genotype and food restriction was present in peak 65B (Fig. 5D, unassigned). Here, source strength was increased in fasted but not in ad libitum fed MC4R-ki mice and reduced in wild type mice in response to fasting.

3.5. Gaussian graphical modelling as a tool to identify VOCs

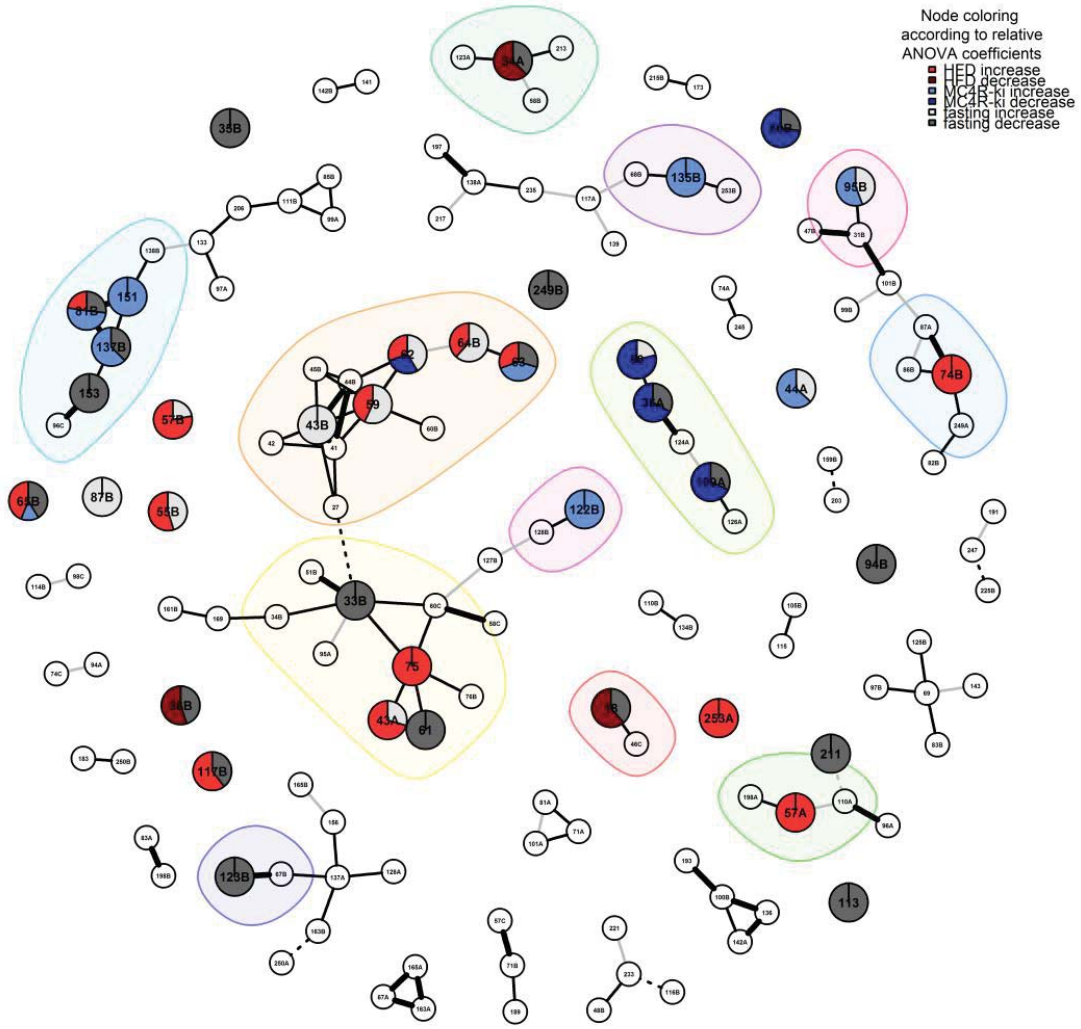

Figure 6: Gaussian graphical model for VOC identification. Gaussian graphical model with nodes corresponding to peaks (labelled with nominal mass and letter for multiple peaks at the same nominal mass) and edges corresponding to shrinkage estimated partial correlation. Highest and lowest 20 percent of correlations are highlighted (bold black/ thin grey). Dotted edges indicate negative partial correlation. Peaks with significant mixed effects model main effects (as seen in Fig. 4 and Fig. 5) are shown as pie charts in nodes. Coloring of model coefficients is according to diet increase/ decrease (red/ dark red), genotype increase/ decrease (blue/ dark blue) and fasting increase/ decrease (grey/ dark grey). Mean fasting coefficients are shown if significant in both obesity models. Subnetworks of peaks with significant effects and directly connected nodes with positive partial correlation are plotted on colored background. Peaks without significant edges selected in AUC-RF were added for illustration purposes.

Gaussian graphical models were proposed recently to identify metabolites and model metabolic pathways from metabolomics data (Krumsiek *et al*, 2012, 2011). As in a large p, smaller n dataset a

full partial correlation matrix cannot be directly applied, we estimated a partial correlation network using a shrinkage approach for longitudinal data (Schäfer & Strimmer, 2005; Opgen-Rhein & Strimmer, 2006). In this graphical model, several obesity relevant subnetworks can be detected with additional information on VOC identity (Fig. 6). In addition to genotype and diet effects, fasting effects are visualized in grey (increase) and dark grey (decrease) pie slices. If both cohorts showed fasting coefficients, we calculated mean coefficients. Fasting coefficients from MC4R cohort contribute to peaks 33B, 35B, 36A, 44A, 61, 62, 63, 65B, 80B, 81B, 87B, 94B, 95B, 109A, 113, 117B, 123B, 137B, 153 and 211 while fasting coefficients from HFD models are contributing to 18, 33B, 34A, 36B, 43A, 43B, 50, 55B, 57B, 59, 62, 64B, 81B and 249B. Interpretations of peak-peak-connections are given in table 1.

Table 1: Tentative assignment of peaks with significant diet, genotype or fasting effects and interpretation of partial correlations to other peaks as depicted in the gaussian graphical model (Fig. 6).

Subnet	peak 1	formula / assignment(s) (mass)	prot. mass	peak 2	formula / assignment(s) (mass)	prot. mass	partial cor.	Interpretation/ pathway
1 / red	18	$NH_3.H^+$ Ammonia (18.03)	18.03	46C	C_2H_7N structure: $CH_3CH_2NH_2.H^+$/ Ethylamine (46.07)	46.06	0.086	(bio)chemical reaction
2 / orange	63	$CO_2.H_3O^+$ / Carbon dioxide water cluster (63.00) $C_2H_6S.H^+$ / Dimethyl sulfide (63.02)	63.01	64B	$^{13}CO_2.\ H_3O^+$ / Carbon dioxide water cluster (64.00) Dimethyl sulfide (64.03) / $^{13}CCH_6S.H^+$	64.01	0.081	C-13 Carbon isotope
	62	$CH_3SCH_2.H^+$ / (Methylthio)methanethiol fragment (62.02)	62.02	64B	$CH_3{}^{34}SCH_2.H^+$ / MTMT fragment (64.02)	64.01	0.074	S-34 Sulfur isotope
				44B	$^{13}CCH_3O.H^+$ / propanol fragment (44.07)	44.07	0.077	Both increase in fasting/ morning
				59	$C_3H_6O.H^+$/ acetone (59.05)	59.05	0.083	Both increase in fasting/ morning
	43B	$C_3H_6.H^+$(43.06) / propanol fragment (after –OH loss)	43.07	45B	$C_2H_4O.H^+$ / Acetaldehyde (45.03) $C_3H_8.H^+$ / Propane (45.07)	45.05	0.078	Unknown/ (Bio) chemical reaction
				42	$^{13}CC_2H_4.H^+$ / propanol fragment (42.05)	42.05	0.081	Carbon isotope of other propanol fragment
				27	$C_2H_2.H^+$ (27.02)	27.01	0.084	Fragment
				59	$C_3H_6O.H^+$/ acetone (59.05)	59.05	0.091	(Bio) chemical reaction catalyzed by alcohol dehydrogenase (adh1)
				44B	$^{13}CCH_3O.H^+$ / propanol fragment (44.07)	44.07	0.108	Carbon isotope
				41	$C_3H_4.H^+$/ propadiene, propanol fragment (41.04)	41.05	0.204	Alternative propanol fragment
	59	$C_3H_6O.H^+$ / Acetone (59.05)	59.05	60B	$^{13}CC_2H_6O.H^+$ / acetone (60.05)	60.05	0.077	C-13 Carbon isotope
				62	$CH_3SCH_2.H+$ / (Methylthio)methanethiol fragment (62.02)	62.02	0.083	Both increase in fasting/ morning
				41	$C_3H_4.H^+$/ propadiene, propanol fragment (41.04)	41.05	0.089	(Bio) chemical reaction catalyzed by alcohol dehydrogenase (adh1)
				43B	$C_3H_6.H^+$(43.06) / propanol fragment (after –OH loss)	43.07	0.091	(Bio) chemical reaction catalyzed by alcohol dehydrogenase (adh1)

				44B	$^{13}CCH_6.H^+$ / propanol fragment (44.07)	44.07	0.094	(Bio) chemical reaction catalyzed by alcohol dehydrogenase (adh1)
				45B	$C_2H_4O.H^+$ / acetaldehyde (45.03) $C_3H_8.H^+$ / Propane (45.07)	45.05	0.096	(Bio) chemical reaction/ unknown
3 / yellow	75	$C_3H_6O_2.H^+$ Methyl acetate (75.04)	75.03	43A	$C_2H_3O^+$ / acylium ion (43.02)	43.03	0.087	Acetate fragment (-H_2O loss)
				61	$C_2H_4O_2.H^+$ / acetic acid (61.03)	61.03	0.090	Biochemical pathway / chemical reaction product / educt
				33B	$CH_3OH.H^+$ / methanol (33.03)	33.04	0.090	Biochemical pathway / chemical reaction product / educt
				60C	$C_3H_9N.H^+$ / Trimethylamine (60.08)	60.08	0.093	High in chow ad libitum / Both can be affected in presence of urine, e.g. during cleaning behavior
				76B	$^{13}CC_2H_6O_2.H^+$ / Methyl acetate (76.02)	76.02	0.095	Carbon isotope
	61	$C_2H_4O_2.H^+$ / acetic acid (61.03)	61.03	43A	$C_2H_3O^+$ / acylium ion (43.02)	43.03	0.157	Acetate fragment (-H_2O loss)
	33B	$CH_3OH.H^+$ / methanol (33.03)	33.04	95A	$C_2H_6S_2.H^+$ / dimethyl sulfone (94.99)	94.96	0.076	Both high in chow ad libitum / methyl group fragmentation
				27	$C_2H_2.H^+$ / fragment of propanol (27.02)	27.01	-0.079	Inverse response to fasting in propanol & acetone subnetwork (2) / possible reaction to propanol
				75	$C_3H_6O_2.H^+$ / Methyl acetate (75.04)	75.03	0.090	(Bio) chemical reaction
				60C	$C_3H_7O.H^+$ / ? (60.06) $C_3H_9N.H^+$ / Trimethylamine (60.08)	60.08	0.096	Both high in chow ad libitum / Can be affected in presence of urine, e.g. during cleaning behavior
				34B	$^{13}CH_3OH.H^+$ / methanol (34.04)	34.05	0.095	Carbon isotope
				51B	$CH_3OH.H_3O^+$ / methanol water cluster (51.05)	51.05	0.113	Water cluster formation
4 /olive green	50	Not assigned	50.01	36A	Not assigned	36.04	0.090	Relation unknown
	36A	Not assigned	36.04	50	Not assigned	50.01	0.090	Relation unknown
				124A	Not assigned	123.84	0.108	Relation unknown
	109A	Not assigned	108.87	124A	Not assigned	123.84	0.074	Relation unknown
				126A	Not assigned	126??	0.078	Relation unknown
5 / green	57A	Not assigned	56.94	110A	Not assigned	109.87	0.074	Relation unknown
				198A	Not assigned	197.65	0.079	Relation unknown
6 / aquamarine	34A	$^{17}O_2$ / oxygen isotope (34.00)	34.00	123A	Not assigned	122.85	0.078	Relation unknown
				213	Not assigned	213.94	0.078	Relation unknown
				58B	$C_2H_3NO.H^+$ (58.03) $CH_3N_3.H^+$ (58.04) $C_3H_5O.H^+$ (58.04)	58.03	0.076	Relation unknown
7 / cyan	81B	Not assigned (pot. $C_4H_4N_2.H^+$ / Pyrazine (81.05), $C_6H_8.H^+$ / hexenal fragment / monoterpene fragment (81.07))	81.04	151	Not assigned (pot. $C_{10}H_{14}O$ (151.10))	150.99	0.099	Relation unknown
				137B	Not assigned (pot. $C_{10}H_{16}.H^+$ / Monoterpenes (137.14))	137.00	0.112	Relation unknown
	151	Not assigned (pot. $C_{10}H_{14}O$ (151.10))	151.00	138B	Not assigned	138.01	0.080	Relation unknown
				137B	Not assigned (pot.	137.00	0.094	Relation unknown

					$C_{10}H_{16}.H^+$ / Monoterpenes (137.14))			
				81B	Not assigned (pot. $C_4H_4N_2.H^+$ / Pyrazine (81.05), $C_6H_8.H^+$ / monoterpene fragment (81.07))	81.04	0.099	Relation unknown
	153	Not assigned (pot. $C_{10}H_{16}O$ (153.12))	152.99	137B	Not assigned (pot. $C_{10}H_{16}.H^+$ / Monoterpenes (137.14))	137.00	0.088	Relation unknown
				96C	Not assigned	95.97	0.098	Relation unknown
	137B	Not assigned (pot. $C_{10}H_{16}.H+$ / Monoterpenes (137.14))	137.00	153	Not assigned (pot. $C_{10}H_{16}O$ (153.12))	152.99	0.088	Relation unknown
				151	Not assigned (pot. $C_{10}H_{14}O$ (151.10))	151.00	0.094	Relation unknown
				81B	Not assigned (pot. $C_4H_4N_2.H^+$ / Pyrazine (81.05), $C_6H_8.H+$ / hexenal fragment / monoterpene fragment (81.07))	81.04	0.112	Relation unknown
8 / blue	74B	Not assigned (pot. C_2H_3NS (74.01))	74.00	249A	Not assigned	248.61	0.079	Relation unknown
				86B	Not assigned ($C_3H_3NO_2$ (86.02))	86.02	0.095	Relation unknown
				87A	Not assigned (86B C-Isotope)	87.00	0.106	Relation unknown
9 / dark blue	123B	Not assigned ($C_7H_6O_2.H^+$ / Benzoic acid (123.04))	123.00	67B	$C_3H_2N_2.H^+$ (67.03) $C_5H_6.H^+$ (67.05)	67.04	0.131	Relation unknown
10 / purple	135B	Not assigned	134.98	68B	Not assigned (pot. $C_4H_5N.H^+$ (68.05))	68.05	0.077	Relation unknown
				253B	Not assigned	252.96	0.081	Relation unknown
11 / light pink	122B	Not assigned	121.98	128B	Not assigned	128.01	0.087	Relation unknown
12 / pink	95B	Not assigned (pot. $C_6H_6O.H^+$ e.g. Phenol (95.05) / $DMSO_2$ (95.01))	95.04	31B	$CH_2O.H^+$ / Formaldehyde (31.02)	31.02	0.089	Relation unknown
No significant positive connections to other VOCs	211	Not assigned	210.97	110A	Not assigned	109.88	-0.070	Relation unknown
	35B	$CH_3{}^{16}OH.H+$ (35.04)	35.05					
	36B	Not assigned ($NH3.H3O^+$ (36.05))	36.07					
	44A	C_2H_3O (44.03) / $^{13}CCH_2O.H^+$ (44.03)	44.03					
	55B	$H_3O^+.(H_2O)_2$ / Water cluster (55.04) $C_4H_6.H^+$ / butadiene as fragment of aldehydes (55.05)	55.05					
	57B	acrolein (2-propenal, $C_3H_4O.H^+$) (57.03)	57.03					
	65B	Unassigned (pot. $C_2H_6{}^{34}S.H^+$ / DMS sulfur isotope (65.03) $C^{18}OO.H_3O^+$ oxygen isotope (65.01))	65.01					
	80B	Not assigned	80.01					
	87B	Not assigned	87.04					
	94B	Not assigned	94.00					
	113	Not assigned	112.98					
	117B	Not assigned	117.01					
	249B	Not assigned	248.94					
	253A	Not assigned	252.60					

4. Discussion

The success of personalized medicine approaches for metabolic diseases depends on inexpensive and minimally invasive but also sensitive and specific diagnostic tools. The analysis of volatile organic compounds in human breath has the potential to provide such an "easy-access" view on a broad range of metabolic pathways. However, the origin and the link to physiological functions of many volatiles are still unknown thus hindering the implementation of a breath gas screen in clinical settings. Here in this study, we screened breath of obese mice for disease related alterations in VOC patterns under controlled and standardized circumstances. We found that a variety of volatiles were affected in obese mice or varied depending on the feeding status of the animals. For both visualizing and identifying altered patterns of volatile organic compounds, we estimated a gaussian graphical model as a data-driven approach novel in PTR-MS based breath gas analysis. Known from metabolomics studies (Krumsiek *et al*, 2012, 2011), graphical modeling here helped to identify contributions to single peaks; for example, isotopes of MTMT (pk62) and $CO_2.H_3O^+$/DMS (pk63) to peak 64B. In addition, visualizing fragmentation patterns like propanol fragments at peaks 41 and 43B is possible (Schwarz *et al*, 2009). In addition to chemical properties, biochemical pathway information could be included, as e.g. the conversion of acetone to 2-propanol by ADH1 (Lewis *et al*, 1984). The combination of this information can shed light on previously unknown peaks and the corresponding volatiles. In addition, the graphical model resembles the hierarchical clustering shown in the two heatmaps in several edges but emphasizes numerous further connections as it can be built on both complete data sets with correction for intra-experimental effects. In the following, the tentatively identified volatiles altered in obese mice are discussed individually with a special emphasis on the available obesity and metabolic disease relevant literature.

4.1. A VOC signature altered in the volatilome both obesity models

In the present study we found that in both diet-induced and genetically induced obesity source strengths of several emitted VOCs were altered. Interestingly, a set of eight peaks was changed in both obesity models, of which four were tentatively identified and four remain unknown.

4.1.1. **Acetic acid (pk61, pk43A)**

A volatile identified in both groups by the feature selection algorithm as potentially relevant was acetic acid (pk61 and fragment pk43A in HFD mice). In this untargeted screening approach mixed effects modeling did not find significantly changed source strengths in acetate but in the fragment

pk43A in HFD mice (pk61 p_{MC4R} = 0.27, p_{HFD} = 0.12; pk43A p_{HFD} = 0.015). Interestingly, despite the non-significant increase in source strength the increased variance and outlying data in both obesity models might be used for stratification of obesity related pathologies like disturbances in glucose homeostasis. The enzymes acetyl-CoA synthetase and acetyl-CoA hydrolase regulate free acetic acid levels, in addition exogenous sources like gut fiber fermentation contribute to serum levels predominantly after food intake (Wolever *et al*, 1997). Serum acetic acid levels were reported to be inversely correlated to insulin levels in mice and humans (Layden *et al*, 2012; Sakakibara *et al*, 2009). Acetate reduces glucose-induced insulin secretion via pancreatic FFAR2 and FFAR3. This is likely mediated by pancreas secreted acetate produced from glucose as a negative feedback as well as from overall systemic acetic acid levels (Tang *et al*, 2015). It is therefore coherent that acetic acid in breath could be used to model glucose levels during an OGTT and to detect individuals with gestational diabetes (Halbritter *et al*, 2012). In addition, short chain fatty acids like acetate have been recognized to induce a PPARγ-dependent switch from lipid synthesis to lipid utilization in white adipose tissue and liver (Besten *et al*, 2015). Thus, if the variance in acetic acid could be attributed to associated (patho)physiological states in obesity, it might be a relevant non-invasive marker.

4.1.2. **Methanol (pk33B)**

Methanol was selected in both models (peaks 33B and MC4R-ki mice also ^{18}O-isotope 35B). A massive increase of methanol was found in the MC4R experiment during the fed state. These mice were fed a so-called chow diet comparably high in pectin/ fiber content thus affecting VOC signatures mediated by altered microbial digestion as previously described (Kistler *et al*, 2014). We could not detect a general effect of obesity status on methanol. Thus, the effect of diet on methanol breath levels seems to exceed the endogenous variation. This is in accordance to other studies, identifying methanol to originate mainly from microbial digestion of consumed pectins with a smaller fraction from other dietary and endogenous sources as aspartame or S-Adenosylmethionine (Axelrod & Daly, 1965; Siragusa *et al*, 1988; Lindinger *et al*, 1997; Dorokhov *et al*, 2012). Notably, methanol was used together with a set of VOCs to model blood glucose in type 1 diabetics (Minh *et al*, 2011) and was found to be reduced in HFD-diet fed rats (Aprea *et al*, 2012), inversely correlated to BMI in humans (Turner *et al*, 2006; Halbritter *et al*, 2012) but increased in liver cirrhosis (Morisco *et al*, 2013). Those findings may be related to differences in life style or eating habits (e.g. reduced fruit (pectin) consumption) affecting gut microbiota in obese patients. In addition, a reduction of methanol detoxification capacity could be present in those states. However, to verify this in a mouse model, it has to considered that detoxification of methanol in humans is primarily adh1 driven, while

in rodents, peroxidative activity of catalase is relevant for degradation (Dorokhov *et al*, 2015; Karinje & Ogata, 1990).

4.1.3. **Carbon dioxide *H_2O / Dimethyl sulfide (pk63, pk64B, pk65)**

Another peak elevated in both obese models is peaks 63 as well as isotopes at 64B (in HFD mice) and probably 65, which are probably a mixed signal from carbon dioxide - water cluster and dimethyl sulfide. Carbon dioxide, as a terminal mitochondrial oxidation product of most energy-containing molecules, is directly related to the amount of energy used in the organism. Indeed the utilized obese models do have an increased overall amount of metabolic active tissue (Figure 1). This increase consists not only of fat mass, which is considered to have a lower but not negligible metabolic activity per gram (Kaiyala *et al*, 2010), but also of highly active lean mass which is elevated. Hence a higher emission of carbon dioxide in heavier mice is not surprising (Butler & Kozak, 2010; Tschöp *et al*, 2012).

DMS, the second candidate, was found to be increased in obese rats with steatohepatitis, obese children, liver cirrhotic patients and is a known constituent of the fetor hepaticus (Aprea *et al*, 2012; Alkhouri *et al*, 2015; Morisco *et al*, 2013; Van den Velde *et al*, 2008). DMS can be found in breath after methionine ingestion and is altered in hepatitis and cirrhosis patients showing an increased half-life (Kaji *et al*, 1979). Furthermore, rat skeletal muscle cells were observed to be releasing DMS, possibly produced by the transamination pathway out of methionine and cysteine (Mochalski *et al*, 2014). Thus, after further insight in its metabolism, DMS could be used as a non-invasive biomarker of altered systemic or hepatic metabolism of sulfur containing amino acids.

4.1.4. **(Methylthio)methanethiol (MTMT, pk62)**

The source strength of a fragment of (methylthio)methanethiol (MTMT, pk62 and part of pk64B signal in HFD fed mice) is ~100 times higher in male mice compared to females (as shown for MC4R-ki animals in Appendix 1). This long-distance pheromone was initially described to be detected in the main olfactory bulb, being involved in the attractiveness of male urine to female mice and can be reduced in urine by castrating male mice (Da Yu Lin *et al*, 2005). Unexpectedly, we found the source strength of MTMT significantly increased in ad libitum fed diet-induced obese mice but reduced in MC4R-ki mice. The tissue and mechanism of endogenous MTMT synthesis are currently unknown. However, a link between the melanocortin 4 receptor and sexual reproduction has been shown (Van

521 der Ploeg *et al*, 2002) and reduced mating success is observed in models with reduction in
522 melanocortin production (Faulkner *et al*, 2015). In contrast to the MC4R-ki mice, upon HFD feeding
523 an elevation in MTMT in ad libitum state but not in the fasted state is observed. Upon HFD feeding,
524 an acute compensatory activation of MC4R signaling is known (Butler *et al*, 2001) and could also
525 modulate MTMT levels via a MC4R-dependent mechanism.

526

527 **4.2. Significant HFD specific peaks**

528

529 4.2.1. **Ammonia (pk18)**

530

531 Ammonia is elevated in liver pathologies (Adeva *et al*, 2012) and was found increased in obese
532 children (Alkhouri *et al*, 2015). In addition, in a rat study featuring diet-induced obesity measured
533 with similar instrumentation, breath ammonium was increased in purified HFD versus low fat
534 standard diet fed rats (Aprea *et al*, 2012). Unexpectedly, we found reduced breath ammonia source
535 strength of in HFD-fed mice in comparison to control mice. Generally, values from HFD-fed mice
536 seem to be lower than both groups in the MC4R experiment as well. In the field of breath research,
537 the reproducibility of breath ammonia measurements is in discussion (Blanco Vela & Bosques
538 Padilla, 2011), as aside from changed blood ammonia concentrations, breath ammonia altered by
539 physical activity level (Solga *et al*, 2014), mode of breathing, airway or mouth pH (Solga *et al*, 2013)
540 and mouth bacteria expressing urease (Chen *et al*, 2014). As mice show a strong preference for nasal
541 breathing, some of the above mentioned effects should not be present here. A higher dietary
542 protein load in this particular HFD (24.1 % in HFD versus 20.8 % in LFD) can contribute to a metabolic
543 acidosis. This in combination with the ketoacidosis in ad libitum HFD and fasting could lead to an
544 increased urinary ammonia excretion to compensate acidosis and therefore reduced breath
545 ammonia.

546

547 4.2.2. **Acrolein (pk57B)**

548 Interestingly, another VOC increased in HFD fed mice both in ad libitum as well as in fasted state but
549 not selected as relevant in MC4R-ki mice is likely acrolein. In humans, acrolein exposure from
550 exogenous sources as diet as well as inhalation of polluted air and smoking are known to be
551 relevant. In addition, endogenous production from lipid peroxidation in oxidative stress, degradation
552 of methionine/ threonine and spermine/ spermidine can contribute to the observed concentrations
553 (Stevens & Maier, 2008). Notably, in HFD mice a slight reduction in fasted state is observed, probably

indicating that both directly diet-derived and endogenous produced acrolein contribute to the elevation compared to LFD fed littermates. Acrolein is contributing to metabolic pathologies via a wide range of mechanisms and target tissues, including protein adduction, induction of oxidative stress, mitochondrial dysfunction, inflammation and immune alterations, ER stress, structural and membrane effects and deregulated signal transduction as reviewed by Moghe et al. (Moghe *et al*, 2015). Hence it can be an interesting breath resource for monitoring carbonyl stress and redox state.

4.2.3. **Methyl acetate (pk75)**

An increase in pk75 in HFD mice was observed, which is possibly predominantly methyl acetate as suggested by the gaussian graphical model. In addition to the individually discussed literature on acetate and methanol, methyl acetate in breath is only described to be increased acutely after exercise (King *et al*, 2010). In obese patients with non-alcoholic fatty liver disease, an increase in various fecal volatile esters including methyl acetate could be observed and associated to a gut microbial shift (Raman *et al*, 2013). Emitted methyl acetate therefore indicates such a shift, or alternatively can be created from acetate and methanol within the mouse metabolism.

4.2.4. **$^{18}O^{16}O$ oxygen (pk34A)**

An increased consumption of oxygen isotope ^{18}O-^{16}O is observed in HFD fed mice. This can likely be explained by a higher amount of metabolic active tissue and therefore higher absolute oxygen demand in the heavier HFD mice (Tschöp *et al*, 2012).

4.2.5. **$H_3O^+.(H_2O)_2$ water cluster and fragments of aldehydes (pk55B)**

Pk55B is increased in HFD mice and is likely to consist of both $H_3O^+.(H_2O)_2$ water cluster and fragments of aldehydes e.g. butanal, hexanal, octanal or nonanal (Buhr *et al*, 2002). Although it is unclear why humidity and water clustering should be increased in obese mice, aldehydes in breath (and breath condensate) can be increased in oxidative stress pathologies with associated lipid peroxidation (Amann *et al*, 2014), which can be elevated in obese state.

4.2.6. **Acetone and propanol (pk59, pk43B)**

In HFD induced obesity, energy demands are to an extended portion satisfied by lipid oxidation and hepatic ketogenesis. One of the ketone bodies is acetone, which is thought to be produced by spontaneous decarboxylation of acetoacetate. Therefore, in both states of increased fatty acid oxidation, namely HFD and food restriction, acetone source strengths are elevated. In humans, fasting breath acetone levels were shown to be highly correlated to ß-hydroxybutyrate and acetoacetate blood concentrations (Qiao *et al*, 2014; Musa-Veloso *et al*, 2006). Both were associated to increased fasting and 2h plasma glucose levels and acetoacetate could be used to predict both an increased GTT AUC and 5-year diabetes incidence (Mahendran *et al*, 2013). Notably, in a subnetwork of fasting responsive volatiles (Figure 6), acetone showed a significant partial correlation to both propanol fragments at nominal masses 41 and 43B (which showed a significant fasting but no diet effect (p=0.118)). The conversion from acetone to iso-propanol is known and can be enhanced in a ketogenic setting (Lewis *et al*, 1984; Petersen *et al*, 2012). As conversion from propanol to acetone is also possible and breath propanol is highly correlated to environmental concentrations in a clinical setting (Ghimenti *et al*, 2013), this can be one reason why in human breath analysis high variance in acetone levels is observed.

4.3. MC4R-ki specific peaks

4.3.1. **Cluster of unknowns 151 (F), 153 (G), 137B (N) and 81B (C)**

In the gaussian graphical model, a subnetwork affected in MC4R-ki mice was observed, featuring peaks 151 (F), 153 (G), 137B (N) and 81B (C). A literature search on similar PTR-MS fragmentation patterns revealed that monoterpenes like α- and β-pinene, 3-carene, limonene and camphor produced fragment ions of masses 67, 81 and 95 as well as a protonated molecular ion of mass 137 or 153 (Tani *et al*, 2003). Notably, in an human lipid infusion study to predict plasma TG and FFA levels from breath volatiles, β-Limonene and β-pinene were relevant for the models (Minh *et al*, 2012). Also monoterpenes (137.137) and terpene-related peak (135.119) have been found as breath markers for liver cirrhosis in a human study (Morisco *et al*, 2013). An altered diet composition as one explanation the authors named can be excluded here. So either increased food consumption in MC4R-ki mice or the suggested alteration hepatic terpene metabolism in this study can explain the elevated levels in obese mice. However, it has to be noted that the observed peaks do not match exactly the theoretical masses. Possibly, the fact that those peaks are far from the internal calibration masses typically applied in PTR-MS measurements using $H_3{}^{18}O^+$ (21.02), NO^+ (30.00) and protonated acetone (59.05) should be causing this mass shift. Especially in the used PTR-TOF-2000

instrument with a resolution of <= 2000 m/Δm, an added high molecular internal calibration gas can be useful to be included in future studies.

4.4. Unassigned volatiles

In addition, three further volatiles - namely peaks 50, 81B and 117B - were identified to be altered in both obese mouse models. Unidentified peaks were also found in HFD fed mice, including peaks 249B, 253A, 57A, 36B and 74B. Even more volatiles are considered unknown in MC4R-ki mice, including peaks 44A, 123B, 135B, 36A, 122B, 137B, 113, 94B, 80B, 87B, 211 and 95B. Those candidates are worth further exploration using complementary methods like classical pre-concentration combined with GC-MS-MS or a novel combination of a fast-GC device to the PTR-MS for additional chemical information (Romano *et al*, 2014). However, altered experimental settings leading to increased VOC concentration can be necessary due to the lower sensitivity of those methods. Alternatively, a nose mask sampling could be applied despite its obvious need for extensive acclimation of rodents to avoid stress induced effects on the measured volatiles (Aprea *et al*, 2012). Interestingly, data-driven models like the applied gaussian graphical model can at least in part contribute to the identification of VOCs. In addition to the volatiles showing effects in mixed effects models, peaks 126A and 48B did not show effects and are considered false positives in the selection process.

5. Conclusion

In this study we characterized alterations in exhaled volatile organic compounds in both diet-induced and mono-genetic obese mouse models and to evaluate whether a common pattern of VOCs altered in obesity can be determined. Alterations in the volatilome could be detected with a common obesity VOC signature. Notably, different adiposity models do create distinct shifts in the volatilome as well, thus showing the potential of VOC analysis to monitor and distinguish different obesogenic mechanisms. Identified VOCs originate from various metabolic pathways and biological processes including ketone body metabolism, lipid peroxidation and pheromones allowing a broad overview over metabolic state in a fast a non-invasive way. In addition, we suggest gaussian graphical models as a helpful tool in understanding and characterizing the volatilome. Thus, the

647 analysis of the volatile metabolome has the potential to contribute to a personalized medicine by
648 aiding in the stratification of patients with heterogeneous metabolic phenotypes and risk profiles.

649

650 ## 6. Conflicts of Interest

651

652 The authors declare that they have no conflict of interest.

653

654 ## 7. Author contributions

655

656 M. Ki. conceived and designed the experiments, researched data, reviewed and analyzed the data
657 and wrote the manuscript. N.R. and A.M. took care of animal management, researched data (A.M.),
658 reviewed and edited the manuscript. W.S. and J.R. conceived and designed the experiments,
659 reviewed the data, wrote (JR), reviewed and edited the manuscript. W.W. contributed to mouse line
660 generation. C.H., M. Kl., H.F., V.GD., W.W. and M.H.A. contributed to discussion, reviewed and
661 edited the manuscript.

662

663 ## 8. Acknowledgments

664

665 We thank Brigitte Herrmann, Ann Elisabeth Schwarz and all animal caretakers in the GMC for their
666 technical contribution to mouse care and phenotyping. Furthermore, our thanks go to Florian Bolze
667 and Ralf Kühn, who contributed to generation and initial characterization of the MC4R-ki mouse line.
668 This work was partly funded by the FP7 Marie Curie Initial Training Network PIMMS, Grant
669 Agreement No. 287382, by German Federal Ministry of Education and Research (Infrafrontier grant
670 01KX1012) and by the German Center for Diabetes Research (DZD).

671

9. References

Adeva MM, Souto G, Blanco N & Donapetry C (2012) Ammonium metabolism in humans. *Metabolism.* **61:** 1495–1511

Alkhouri N, Cikach F, Eng K, Moses J, Patel N, Yan C, Hanouneh I, Grove D, Lopez R & Dweik R (2014) Analysis of breath volatile organic compounds as a noninvasive tool to diagnose nonalcoholic fatty liver disease in children: *Eur. J. Gastroenterol. Hepatol.* **26:** 82–87

Alkhouri N, Eng K, Cikach F, Patel N, Yan C, Brindle A, Rome E, Hanouneh I, Grove D, Lopez R, Hazen SL & Dweik RA (2015) Breathprints of childhood obesity: changes in volatile organic compounds in obese children compared with lean controls. *Pediatr. Obes.* **10:** 23–29

Amann A, Miekisch W, Schubert J, Buszewski B, Ligor T, Jezierski T, Pleil J & Risby T (2014) Analysis of Exhaled Breath for Disease Detection. *Annu. Rev. Anal. Chem.* **7:** 455–482

Aprea E, Morisco F, Biasioli F, Vitaglione P, Cappellin L, Soukoulis C, Lembo V, Gasperi F, D'Argenio G, Fogliano V & Caporaso N (2012) Analysis of breath by proton transfer reaction time of flight mass spectrometry in rats with steatohepatitis induced by high-fat diet. *J. Mass Spectrom. JMS* **47:** 1098–1103

Axelrod J & Daly J (1965) Pituitary gland: enzymic formation of methanol from S-adenosylmethionine. *Science* **150:** 892–893

Baranska A, Tigchelaar E, Smolinska A, Dallinga JW, Moonen EJC, Dekens JAM, Wijmenga C, Zhernakova A & van Schooten FJ (2013) Profile of volatile organic compounds in exhaled breath changes as a result of gluten-free diet. *J. Breath Res.* **7:** 037104

Basanta M, Ibrahim B, Douce D, Morris M, Woodcock A & Fowler SJ (2012) Methodology validation, intra-subject reproducibility and stability of exhaled volatile organic compounds. *J. Breath Res.* **6:** 026002

Benjamini Y & Hochberg Y (1995) Controlling the False Discovery Rate: A Practical and Powerful Approach to Multiple Testing. *J. R. Stat. Soc. Ser. B Methodol.* **57:** 289–300

Besten G den, Bleeker A, Gerding A, van Eunen K, Havinga R, van Dijk TH, Oosterveer MH, Jonker JW, Groen AK, Reijngoud D-J & Bakker BM (2015) Short-Chain Fatty Acids Protect Against High-Fat Diet–Induced Obesity via a PPARγ-Dependent Switch From Lipogenesis to Fat Oxidation. *Diabetes* **64:** 2398–2408

Blanco Vela CI & Bosques Padilla FJ (2011) Determination of ammonia concentrations in cirrhosis patients-still confusing after all these years? *Ann. Hepatol.* **10 Suppl 2:** S60–65

Bolze F, Rink N, Brumm H, Kühn R, Mocek S, Schwarz A-E, Kless C, Biebermann H, Wurst W, Rozman J & Klingenspor M (2011) Characterization of the melanocortin-4-receptor nonsense mutation W16X in vitro and in vivo. *Pharmacogenomics J.* **13:** Available at: http://www.readcube.com/articles/10.1038%2Ftpj.2011.43 [Accessed February 23, 2015]

Boots AW, van Berkel JJBN, Dallinga JW, Smolinska A, Wouters EF & van Schooten FJ (2012) The versatile use of exhaled volatile organic compounds in human health and disease. *J. Breath Res.* **6:** 027108

Buhr K, van Ruth S & Delahunty C (2002) Analysis of volatile flavour compounds by Proton Transfer Reaction-Mass Spectrometry: fragmentation patterns and discrimination between isobaric and isomeric compounds. *Int. J. Mass Spectrom.* **221:** 1–7

Butler AA & Kozak LP (2010) A Recurring Problem With the Analysis of Energy Expenditure in Genetic Models Expressing Lean and Obese Phenotypes. *Diabetes* **59:** 323–329

Butler AA, Marks DL, Fan W, Kuhn CM, Bartolome M & Cone RD (2001) Melanocortin-4 receptor is required for acute homeostatic responses to increased dietary fat. *Nat. Neurosci.* **4:** 605–611

van Buuren S & Groothuis-Oudshoorn K (2011) mice: Multivariate Imputation by Chained Equations in R. *J. Stat. Softw.* **45:** 1–67

Chang W, Cheng J, Allaire JJ, Xie Y, McPherson J, RStudio, library) jQuery F (jQuery library and jQuery U, ininst/www/shared/jquery-AUTHORS.txt) jQuery contributors (jQuery library; authors listed, ininst/www/shared/jqueryui/1.10.4/AUTHORS.txt) jQuery U contributors (jQuery U library; authors listed, library) MO (Bootstrap, library) JT (Bootstrap, library) B contributors (Bootstrap, Twitter, library) I (Bootstrap, library) AF (html5shiv, library) SJ (Respond js, library) SP (Bootstrap-datepicker, library) AR (Bootstrap-datepicker, font) DG (Font-A, library) BR (selectize js, et al (2015) shiny: Web Application Framework for R Available at: http://cran.r-project.org/web/packages/shiny/index.html [Accessed February 11, 2015]

Chen W, Metsälä M, Vaittinen O & Halonen L (2014) The origin of mouth-exhaled ammonia. *J. Breath Res.* **8:** 036003

Dorokhov YL, Komarova TV, Petrunia IV, Kosorukov VS, Zinovkin RA, Shindyapina AV, Frolova OY & Gleba YY (2012) Methanol May Function as a Cross-Kingdom Signal. *PLoS ONE* **7:** Available at: http://www.ncbi.nlm.nih.gov/pmc/articles/PMC3338578/ [Accessed July 19, 2013]

Dorokhov YL, Shindyapina AV, Sheshukova EV & Komarova TV (2015) Metabolic Methanol: Molecular Pathways and Physiological Roles. *Physiol. Rev.* **95:** 603–644

Elliott P, Posma JM, Chan Q, Garcia-Perez I, Wijeyesekera A, Bictash M, Ebbels TMD, Ueshima H, Zhao L, van Horn L, Daviglus M, Stamler J, Holmes E & Nicholson JK (2015) Urinary metabolic signatures of human adiposity. *Sci. Transl. Med.* **7:** 285ra62–285ra62

Faulkner L, Dowling A, Stuart R, Nillni E & Hill J (2015) Reduced melanocortin production causes sexual dysfunction in male mice with POMC neuronal insulin and leptin insensitivity. *Endocrinology***:** en.2014–1788

Fink T, Wolf A, Maurer F, Albrecht FW, Heim N, Wolf B, Hauschild AC, Bödeker B, Baumbach JI, Volk T, Sessler DI & Kreuer S (2014) Volatile Organic Compounds during Inflammation and Sepsis in Rats: A Potential Breath Test Using Ion-mobility Spectrometry. *Anesthesiology*

Fuchs H, Gailus-Durner V, Adler T, Pimentel JAA, Becker L, Bolle I, Brielmeier M, Calzada-Wack J, Dalke C, Ehrhardt N, Fasnacht N, Ferwagner B, Frischmann U, Hans W, Hölter SM, Hölzlwimmer G, Horsch M, Javaheri A, Kallnik M, Kling E, et al (2009) The German Mouse Clinic: a platform for systemic phenotype analysis of mouse models. *Curr. Pharm. Biotechnol.* **10:** 236–243

Gentleman RC, Carey VJ, Bates DM & others (2004) Bioconductor: Open software development for computational biology and bioinformatics. *Genome Biol.* **5:** R80

751 Ghimenti S, Tabucchi S, Lomonaco T, Di Francesco F, Fuoco R, Onor M, Lenzi S & Trivella MG (2013)
752 Monitoring breath during oral glucose tolerance tests. *J. Breath Res.* **7:** 017115

753 Greiter MB, Keck L, Siegmund T, Hoeschen C, Oeh U & Paretzke HG (2010) Differences in exhaled gas
754 profiles between patients with type 2 diabetes and healthy controls. *Diabetes Technol. Ther.*
755 **12:** 455–463

756 Guh DP, Zhang W, Bansback N, Amarsi Z, Birmingham CL & Anis AH (2009) The incidence of co-
757 morbidities related to obesity and overweight: A systematic review and meta-analysis. *BMC*
758 *Public Health* **9:** 88

759 Halbritter S, Fedrigo M, Höllriegl V, Szymczak W, Maier JM, Ziegler A-G & Hummel M (2012) Human
760 Breath Gas Analysis in the Screening of Gestational Diabetes Mellitus. *Diabetes Technol.*
761 *Ther.* Available at: http://www.ncbi.nlm.nih.gov/pubmed/22775148 [Accessed July 12, 2012]

762 Hothorn T, Bretz F, Westfall P, Heiberger RM & Schuetzenmeister A (2014) multcomp: Simultaneous
763 Inference in General Parametric Models Available at: http://cran.us.r-
764 project.org/web/packages/multcomp/index.html [Accessed February 10, 2015]

765 Kaiyala KJ, Morton GJ, Leroux BG, Ogimoto K, Wisse B & Schwartz MW (2010) Identification of Body
766 Fat Mass as a Major Determinant of Metabolic Rate in Mice. *Diabetes* **59:** 1657–1666

767 Kaji H, Hisamura M, Saito N, Sakai H, Aikawa T, Kondo T, Ide H & Murao M (1979) Clinical application
768 of breath analysis for dimethyl sulfide following ingestion of DL-methionine. *Clin. Chim. Acta*
769 *Int. J. Clin. Chem.* **93:** 377–380

770 Karinje KU & Ogata M (1990) Methanol metabolism in acatalasemic mice. *Physiol. Chem. Phys. Med.*
771 *NMR* **22:** 193–198

772 King J, Mochalski P, Kupferthaler A, Unterkofler K, Koc H, Filipiak W, Teschl S, Hinterhuber H &
773 Amann A (2010) Dynamic profiles of volatile organic compounds in exhaled breath as
774 determined by a coupled PTR-MS/GC-MS study. *Physiol. Meas.* **31:** 1169

775 Kistler M, Szymczak W, Fedrigo M, Fiamoncini J, Höllriegl V, Hoeschen C, Klingenspor M, Hrabě de
776 Angelis M & Rozman J (2014) Effects of diet-matrix on volatile organic compounds in breath
777 in diet-induced obese mice. *J. Breath Res.* **8:** 016004

778 Koeth RA, Wang Z, Levison BS, Buffa JA, Org E, Sheehy BT, Britt EB, Fu X, Wu Y, Li L, Smith JD,
779 DiDonato JA, Chen J, Li H, Wu GD, Lewis JD, Warrier M, Brown JM, Krauss RM, Tang WHW, et
780 al (2013) Intestinal microbiota metabolism of L-carnitine, a nutrient in red meat, promotes
781 atherosclerosis. *Nat. Med.* **19:** 576–585

782 Krumsiek J, Suhre K, Evans AM, Mitchell MW, Mohney RP, Milburn MV, Wagele B, Romisch-Margl W,
783 Illig T, Adamski J, Gieger C, Theis FJ & Kastenmuller G (2012) Mining the Unknown: A
784 Systems Approach to Metabolite Identification Combining Genetic and Metabolic
785 Information. *PLoS Genet.* **8:** Available at:
786 http://www.ncbi.nlm.nih.gov/pmc/articles/PMC3475673/ [Accessed July 31, 2013]

787 Krumsiek J, Suhre K, Illig T, Adamski J & Theis FJ (2011) Gaussian graphical modeling reconstructs
788 pathway reactions from high-throughput metabolomics data. *BMC Syst. Biol.* **5:** 21

Layden BT, Yalamanchi SK, Wolever TM, Dunaif A & Lowe WL (2012) Negative association of acetate with visceral adipose tissue and insulin levels. *Diabetes Metab. Syndr. Obes. Targets Ther.* **5:** 49–55

Lee J, Ngo J, Blake D, Meinardi S, Pontello AM, Newcomb R & Galassetti PR (2009) Improved predictive models for plasma glucose estimation from multi-linear regression analysis of exhaled volatile organic compounds. *J. Appl. Physiol.* **107:** 155 –160

Lewis GD, Laufman AK, McAnalley BH & Garriott JC (1984) Metabolism of acetone to isopropyl alcohol in rats and humans. *J. Forensic Sci.* **29:** 541–549

Lindinger W, Hansel A & Jordan A (1998) On-line monitoring of volatile organic compounds at pptv levels by means of proton-transfer-reaction mass spectrometry (PTR-MS) medical applications, food control and environmental research. *Int. J. Mass Spectrom. Ion Process.* **173:** 191–241

Lindinger W, Taucher J, Jordan A, Hansel A & Vogel W (1997) Endogenous Production of Methanol after the Consumption of Fruit. *Alcohol. Clin. Exp. Res.* **21:** 939–943

Mahendran Y, Vangipurapu J, Cederberg H, Stančáková A, Pihlajamäki J, Soininen P, Kangas AJ, Paananen J, Civelek M, Saleem NK, Pajukanta P, Lusis AJ, Bonnycastle LL, Morken MA, Collins FS, Mohlke KL, Boehnke M, Ala-Korpela M, Kuusisto J & Laakso M (2013) Association of ketone body levels with hyperglycemia and type 2 diabetes in 9,398 Finnish men. *Diabetes* Available at: http://diabetes.diabetesjournals.org/content/early/2013/04/01/db12-1363 [Accessed April 11, 2013]

Martinez-Lozano Sinues P, Tarokh L, Li X, Kohler M, Brown SA, Zenobi R & Dallmann R (2014) Circadian Variation of the Human Metabolome Captured by Real-Time Breath Analysis. *PLoS ONE* **9:** Available at: http://www.ncbi.nlm.nih.gov/pmc/articles/PMC4278702/ [Accessed February 20, 2015]

Minh TDC, Oliver SR, Flores RL, Ngo J, Meinardi S, Carlson MK, Midyett J, Rowland FS, Blake DR & Galassetti PR (2012) Noninvasive Measurement of Plasma Triglycerides and Free Fatty Acids from Exhaled Breath. *J. Diabetes Sci. Technol.* **6:** 86–101

Minh TDC, Oliver SR, Ngo J, Flores R, Midyett J, Meinardi S, Carlson MK, Rowland FS, Blake DR & Galassetti PR (2011) Noninvasive measurement of plasma glucose from exhaled breath in healthy and type 1 diabetic subjects. *Am. J. Physiol. Endocrinol. Metab.* **300:** E1166–1175

Mochalski P, Al-Zoairy R, Niederwanger A, Unterkofler K & Amann A (2014) Quantitative analysis of volatile organic compounds released and consumed by rat L6 skeletal muscle cells *in vitro*. *J. Breath Res.* **8:** 046003

Moghe A, Ghare S, Lamoreau B, Mohammad M, Barve S, McClain C & Joshi-Barve S (2015) Molecular Mechanisms of Acrolein Toxicity: Relevance to Human Disease. *Toxicol. Sci.* **143:** 242–255

Morisco F, Aprea E, Lembo V, Fogliano V, Vitaglione P, Mazzone G, Cappellin L, Gasperi F, Masone S, De Palma GD, Marmo R, Caporaso N & Biasioli F (2013) Rapid 'Breath-Print' of Liver Cirrhosis by Proton Transfer Reaction Time-of-Flight Mass Spectrometry. A Pilot Study. *PloS One* **8:** e59658

828 Musa-Veloso K, Likhodii SS, Rarama E, Benoit S, Liu Y-MC, Chartrand D, Curtis R, Carmant L, Lortie A,
829 Comeau FJE & Cunnane SC (2006) Breath acetone predicts plasma ketone bodies in children
830 with epilepsy on a ketogenic diet. *Nutr. Burbank Los Angel. Cty. Calif* **22:** 1–8

831 Novak BJ, Blake DR, Meinardi S, Rowland FS, Pontello A, Cooper DM & Galassetti PR (2007) Exhaled
832 methyl nitrate as a noninvasive marker of hyperglycemia in type 1 diabetes. *Proc. Natl. Acad.*
833 *Sci.* **104:** 15613 –15618

834 Opgen-Rhein R & Strimmer K (2006) Inferring gene dependency networks from genomic longitudinal
835 data: a functional data approach. *RevStat* **4:** 53–65

836 Petersen TH, Williams T, Nuwayhid N & Harruff R (2012) Postmortem Detection of Isopropanol in
837 Ketoacidosis: POSTMORTEM DETECTION OF ISOPROPANOL IN KETOACIDOSIS. *J. Forensic Sci.*
838 **57:** 674–678

839 Petersson F, Sulzer P, Mayhew CA, Watts P, Jordan A, Märk L & Märk TD (2009) Real-time trace
840 detection and identification of chemical warfare agent simulants using recent advances in
841 proton transfer reaction time-of-flight mass spectrometry. *Rapid Commun. Mass Spectrom.*
842 **23:** 3875–3880

843 Phillips M, Herrera J, Krishnan S, Zain M, Greenberg J & Cataneo RN (1999) Variation in volatile
844 organic compounds in the breath of normal humans. *J. Chromatogr. B. Biomed. Sci. App.*
845 **729:** 75–88

846 Pinheiro J, Bates D, DebRoy S, Deepayan S & R-core (2015) nlme: Linear and Nonlinear Mixed Effects
847 Models Available at: http://cran.us.r-project.org/web/packages/nlme/index.html [Accessed
848 February 10, 2015]

849 Van der Ploeg LHT, Martin WJ, Howard AD, Nargund RP, Austin CP, Guan X, Drisko J, Cashen D,
850 Sebhat I, Patchett AA, Figueroa DJ, DiLella AG, Connolly BM, Weinberg DH, Tan CP, Palyha
851 OC, Pong S-S, MacNeil T, Rosenblum C, Vongs A, et al (2002) A role for the melanocortin 4
852 receptor in sexual function. *Proc. Natl. Acad. Sci. U. S. A.* **99:** 11381–11386

853 Ploner A (2014) Heatplus: Heatmaps with row and/or column covariates and colored clusters

854 Qiao Y, Gao Z, Liu Y, Cheng Y, Yu M, Zhao L, Duan Y & Liu Y (2014) Breath Ketone Testing: A New
855 Biomarker for Diagnosis and Therapeutic Monitoring of Diabetic Ketosis. *BioMed Res. Int.*
856 **2014:** Available at: http://www.ncbi.nlm.nih.gov/pmc/articles/PMC4037575/ [Accessed
857 January 22, 2015]

858 Raman M, Ahmed I, Gillevet PM, Probert CS, Ratcliffe NM, Smith S, Greenwood R, Sikaroodi M, Lam
859 V, Crotty P, Bailey J, Myers RP & Rioux KP (2013) Fecal Microbiome and Volatile Organic
860 Compound Metabolome in Obese Humans With Nonalcoholic Fatty Liver Disease. *Clin.*
861 *Gastroenterol. Hepatol.* **11:** 868–875.e3

862 R Core Team (2014) R: A language and environment for statistical computing. R Foundation for
863 Statistical Computing Vienna, Austria Available at: http://www.R-project.org/

864 Romano A, Fischer L, Herbig J, Campbell-Sills H, Coulon J, Lucas P, Cappellin L & Biasioli F (2014)
865 Wine analysis by FastGC proton-transfer reaction-time-of-flight-mass spectrometry. *Int. J.*
866 *Mass Spectrom.* **369:** 81–86

867 Rosenthal N & Brown S (2007) The mouse ascending: perspectives for human-disease models. *Nat.*
868 *Cell Biol.* **9:** 993–999

869 Sakakibara I, Fujino T, Ishii M, Tanaka T, Shimosawa T, Miura S, Zhang W, Tokutake Y, Yamamoto J,
870 Awano M, Iwasaki S, Motoike T, Okamura M, Inagaki T, Kita K, Ezaki O, Naito M, Kuwaki T,
871 Chohnan S, Yamamoto TT, et al (2009) Fasting-Induced Hypothermia and Reduced Energy
872 Production in Mice Lacking Acetyl-CoA Synthetase 2. *Cell Metab.* **9:** 191–202

873 Schaefer J, Opgen-Rhein R & Strimmer K (2015) GeneNet: Modeling and Inferring Gene Networks
874 Available at: http://CRAN.R-project.org/package=GeneNet

875 Schäfer J, Opgen-Rhein R & Strimmer K (2001) Reverse engineering genetic networks using the
876 GeneNet package. *J Am Stat Assoc* **96:** 1151–1160

877 Schäfer J & Strimmer K (2005) A shrinkage approach to large-scale covariance matrix estimation and
878 implications for functional genomics. *Stat. Appl. Genet. Mol. Biol.* **4:** Available at:
879 http://www.degruyter.com/view/j/sagmb.2005.4.1/sagmb.2005.4.1.1175/sagmb.2005.4.1.1
880 175.xml [Accessed August 21, 2014]

881 Schwarz K, Filipiak W & Amann A (2009) Determining concentration patterns of volatile compounds
882 in exhaled breath by PTR-MS. *J. Breath Res.* **3:** 027002

883 Siragusa RJ, Cerda JJ, Baig MM, Burgin CW & Robbins FL (1988) Methanol production from the
884 degradation of pectin by human colonic bacteria. *Am. J. Clin. Nutr.* **47:** 848–851

885 Solga SF, Mudalel M, Spacek LA, Lewicki R, Tittel FK, Loccioni C, Russo A, Ragnoni A & Risby TH (2014)
886 Changes in the concentration of breath ammonia in response to exercise: a preliminary
887 investigation. *J. Breath Res.* **8:** 037103

888 Solga SF, Mudalel M, Spacek LA, Lewicki R, Tittel F, Loccioni C, Russo A & Risby TH (2013) Factors
889 influencing breath ammonia determination. *J. Breath Res.* **7:** 037101

890 Stevens JF & Maier CS (2008) Acrolein: sources, metabolism, and biomolecular interactions relevant
891 to human health and disease. *Mol. Nutr. Food Res.* **52:** 7–25

892 Szymczak W, Rozman J, Höllriegl V, Kistler M, Keller S, Peters D, Kneipp M, Schulz H, Hoeschen C,
893 Klingenspor M & de Angelis MH (2014) Online breath gas analysis in unrestrained mice by
894 hs-PTR-MS. *Mamm. Genome Off. J. Int. Mamm. Genome Soc.* **25:** 129–140

895 Tang C, Ahmed K, Gille A, Lu S, Gröne H-J, Tunaru S & Offermanns S (2015) Loss of FFA2 and FFA3
896 increases insulin secretion and improves glucose tolerance in type 2 diabetes. *Nat. Med.* **21:**
897 173–177

898 Tani A, Hayward S & Hewitt CN (2003) Measurement of monoterpenes and related compounds by
899 proton transfer reaction-mass spectrometry (PTR-MS). *Int. J. Mass Spectrom.* **223–224:** 561–
900 578

901 Tschöp MH, Speakman JR, Arch JRS, Auwerx J, Brüning JC, Chan L, Eckel RH, Farese Jr RV, Galgani JE,
902 Hambly C, Herman MA, Horvath TL, Kahn BB, Kozma SC, Maratos-Flier E, Müller TD,
903 Münzberg H, Pfluger PT, Plum L, Reitman ML, et al (2012) A guide to analysis of mouse
904 energy metabolism. *Nat. Methods* **9:** 57–63

Turner C, Spanel P & Smith D (2006) A longitudinal study of methanol in the exhaled breath of 30 healthy volunteers using selected ion flow tube mass spectrometry, SIFT-MS. *Physiol. Meas.* **27:** 637–648

Urrea V & Calle ML (2012) AUCRF: Variable Selection with Random Forest and the Area Under the Curve Available at: http://cran.us.r-project.org/web/packages/AUCRF/index.html [Accessed February 10, 2015]

Van den Velde S, Nevens F, Van Hee P, van Steenberghe D & Quirynen M (2008) GC-MS analysis of breath odor compounds in liver patients. *J. Chromatogr. B Analyt. Technol. Biomed. Life. Sci.* **875:** 344–348

Wahl S, Vogt S, Stückler F, Krumsiek J, Bartel J, Kacprowski T, Schramm K, Carstensen M, Rathmann W, Roden M, Jourdan C, Kangas AJ, Soininen P, Ala-Korpela M, Nöthlings U, Boeing H, Theis FJ, Meisinger C, Waldenberger M, Suhre K, et al (2015) Multi-omic signature of body weight change: results from a population-based cohort study. *BMC Med.* **13:** 48

Wickham H (2009) ggplot2: elegant graphics for data analysis Springer New York Available at: http://had.co.nz/ggplot2/book

Wlodzimirow KA, Abu-Hanna A, Schultz MJ, Maas M a. W, Bos LDJ, Sterk PJ, Knobel HH, Soers RJT & Chamuleau RAFM (2014) Exhaled breath analysis with electronic nose technology for detection of acute liver failure in rats. *Biosens. Bioelectron.* **53:** 129–134

Wolever T, Josse RG, Leiter LA & Chiasson J-L (1997) Time of day and glucose tolerance status affect serum short-chain fatty concentrations in humans. *Metabolism* **46:** 805–811

Da Yu Lin S-ZZ, Block E & Katz LC (2005) Encoding social signals in the mouse main olfactory bulb. *Nature* **434:** 470–477

10. Supplements

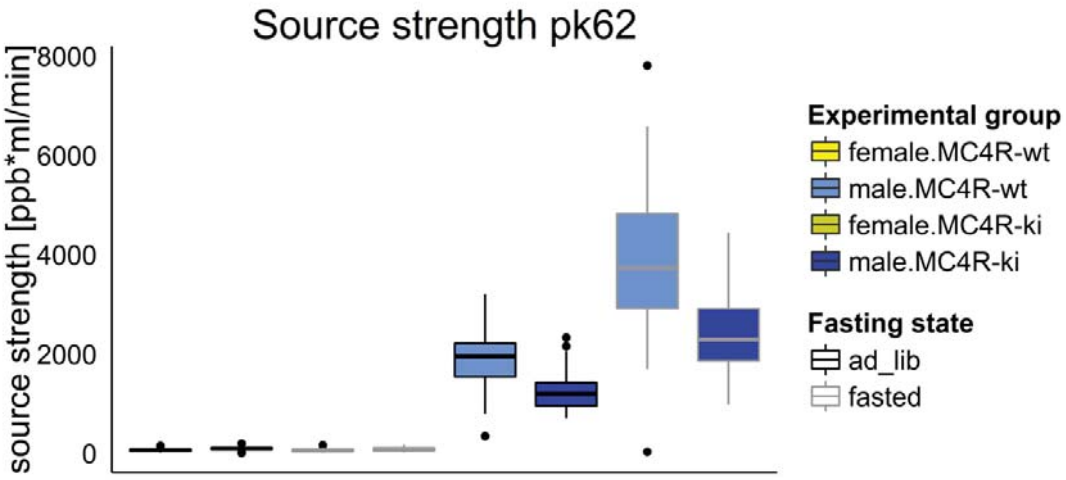

Supplementary figure 1: Source strengths of pk62 in males and females. Source strengths of pk62 (MTMT) are shown as boxplots. Box fill corresponds to genotype and sex (blue: male melanocortin-4-receptor wild type; dark blue: male melanocortin-4-receptor W16X knock-in, yellow: female melanocortin-4-receptor wild type; dark yellow: female melanocortin-4-receptor W16X knock-in). Box border corresponds to fasting state (black: ad libitum fed; grey: fasted).

Supplementary table 1: Linear mixed effects model testing showing genotype, diet and fasting effects on VOC source strengths

peak	fasted								ad libitum fed								Lme diet & fasting status			Posthoc-test diet & fasting status				Lme genotype & fasting status			Posthoc-test genotype & fasting status			
	mean LFD		mean HFD		mean MC4R-wt		mean MC4R-ki		mean LFD		mean HFD		mean MC4R-wt		mean MC4R-ki		diet	feed state	diet: feed state	ad-lib LowFat - ad-lib HighFat	fasted LowFat - ad-lib LowFat	fasted HighFat - ad-lib HighFat	fasted HighFat - fasted LowFat	genotype	feed state	gt: feed state	ad-lib MC4R-ki - ad-lib BL6	ad-lib BL6 - fasted BL6	ad-lib MC4R-ki - fasted MC4R-ki	fasted BL6 - fasted MC4R-ki
	mean	*sd*	mean	*sd*	mean	*sd*	mean	*sd*	mean	*sd*	mean	*sd*	mean	*sd*	mean	*sd*													
pk18	745175.43	385208.81	110462.5	194262.69	930685.55	1149901.07	915767.67	1117265.86	161576.84	45037.2	45369.32	23502.63	132291.94	93456.28	202016.45	99732.22	**2,000E-05**	**2,040E-19**	**4,022E-08**	**1,024E-11**	**0,000E+00**	**1,415E-02**	**7,851E-04**							
pk57B	58.04	23.6	120.54	50.68	56.61	36.15	73.53	45.04	67.17	17.64	91.52	28.7	22.2	16.22	32.85	22.74	**1,183E-04**	**3,147E-02**	**5,167E-04**	1,009E-08	2,723E-02	4,651E-03	4,606E-02							
pk65B	23.4	7.06	35.52	13.5	11.12	4.58	13.38	4.07	30.44	9.26	42.99	12.53	7.88	3.25	13.24	7.15	**5,203E-02**	6,264E-01	6,669E-01					4,181E-01	**1,967E-05**	**1,381E-02**	4,034E-01	**4,347E-06**	7,462E-01	**1,473E-04**
pk63	1566.95	414.1	1958.68	488.37	1012.43	165.48	1438.3	284.57	1687.35	569.59	2302.49	538.94	845.22	202.71	1295.46	255.99	**3,147E-02**	3,763E-01	3,179E-01					**2,057E-03**	**2,625E-05**	**6,754E-02**				
pk75	96.23	31.89	147.73	65.06	185.74	132.46	385.89	257.26	83.12	18.64	117.01	44.55	59.21	49.18	99.84	97.73	**1,415E-02**	1,393E-01	1,474E-01											
pk62	1027.11	408.79	1952.28	576.09	1591.08	533.48	996.38	225.29	2891.28	1115.26	3121.95	929.57	2886.29	911.32	1999.94	693.96	**9,986E-04**	**1,449E-24**	**8,086E-06**	**9,625E-06**	**0,000E+00**	**1,827E-11**	3,818E-01	**8,994E-05**	**1,158E-11**	**7,876E-02**				
pk50	117.52	28.26	93.19	40.42	111.3	91.98	66.2	41.19	144.1	35.54	103.1	47.26	116.03	39.12	90.02	37.87	1,359E-01	**7,131E-02**	3,562E-01					**1,468E-02**	4,775E-01	1,366E-01				
pk249B	0.5	1.72	1.45	1.91	0.14	0.42	0.34	0.52	-0.34	2.2	1.33	2.36	0.18	0.76	0.19	0.81	3,339E-01	**7,131E-02**	3,428E-01											
pk253A	0.64	1.55	2.28	1.83	-0.23	1.24	0	0.54	0.76	2.01	1.98	1.98	0.07	0.64	0.24	0.78	**1,879E-02**	9,004E-01	8,229E-01											
pk117B	6.23	3.72	10.93	4.2	5.46	3.85	6.79	3.67	5.81	4.02	7.66	4.01	2.75	1.67	4.53	2.6	**1,212E-02**	3,763E-01	1,824E-01					3,363E-01	**7,390E-05**	3,806E-01				
pk57A	-0.6	4.53	1.82	4.31	3.28	7.33	2.58	2.16	0.55	5.18	3.4	3.2	1.39	3.05	-0.14	2.2	**9,306E-02**	3,179E-01	9,471E-01											
pk34A	-494.39	119.32	-603.33	115.66	-759.1	337.44	-656.4	137.48	-558.4	117	-665.69	114	-621.17	174.63	-687.96	199.8	**1,879E-02**	**4,472E-02**	9,941E-01											
pk81B	8.22	6.6	12.81	6.72	21.17	30.5	46.02	38.35	5	6.7	8.79	5.49	10.81	11.03	30.1	28.15	**9,306E-02**	**1,306E-02**	5,358E-01					**1,468E-02**	**4,935E-02**	9,177E-01				
pk74B	2.96	3.47	7.52	3.04	9.49	5.09	12.35	4.65	2.93	4.55	4.57	4.63	6.75	3.87	7.43	4.95	**3,358E-02**	4,818E-01	3,428E-01											
pk55B	4999.52	2046.66	7316.99	4020.37	1164.13	851.25	934.84	741.57	7022.74	1540.06	8378.98	2882.74	854.03	608.39	915.28	845.59	**5,203E-02**	**8,484E-04**	2,123E-01											
pk36B	243.9	78.58	176.87	100.91	60.58	48.76	59.34	41.74	189.06	44.65	170.92	35.73	20.57	14.59	26.51	13.75	**2,324E-02**	**1,109E-05**	**6,829E-04**	**7,580E-03**	**2,235E-06**	7,069E-01	7,641E-01							
pk43B	1009.98	920.7	1412.64	598.59	267.05	365.81	461.62	154.96	3062.19	1122.86	4166.27	1187.44	2187.59	1059.13	3850.39	4631.54	1,176E-01	**6,311E-28**	8,814E-01											
pk61	2078.78	855.63	3094.76	1958.12	1246.68	579.7	2040.58	1179.51	2340.07	701.24	3225.45	1473.24	1041.86	463.09	1659.27	918.77	1,215E-01	1,741E-01	6,082E-01					2,678E-01	**6,876E-02**	5,241E-01				
pk43A	1330	544.13	2166.76	1556.78	1048.61	522.98	1511.81	866.94	1599.87	490.29	2224.13	1115.73	994.38	435.81	1538.85	973.67	**8,030E-02**	**3,147E-02**	2,739E-01											
pk33B	1325.42	479.39	1038.93	346.57	10576.25	5966.05	9300.59	4344.93	1443.82	362.2	1339.73	495.97	997.49	391.96	957.04	788.17	2,628E-01	**7,131E-02**	3,523E-01					4,034E-01	**5,809E-41**	9,177E-01				
pk59	252.32	166.83	747.21	639.59	215.81	101.58	232.03	104.25	812.26	321.44	1047.4	371	822.79	501.83	1365.93	1770.97	**3,299E-02**	**2,191E-09**	1,970E-01											
pk64B	17.45	7.11	24.25	8.48	15.65	5.41	19.15	4.03	27.73	9.69	33.42	9	20.48	6.75	21.1	6.06	**4,038E-02**	**1,716E-05**	4,472E-01											
pk123B	5.77	5.29	8.37	5.19	8.6	6.95	9.9	4.26	4.53	5.36	6.39	4.2	4.19	2.97	7.81	4.52								2,678E-01	**8,994E-05**	3,128E-01				
pk151	4.09	4.01	6.65	4.44	8.03	13.06	16.52	15.42	3.83	3.13	5.67	3.64	4.38	5.59	13.2	14.35								**4,154E-02**	1,740E-01	7,462E-01				
pk153	4.84	4.26	5.72	4.52	4.91	6.89	6.46	5.05	3.22	4.47	4.08	3.43	2.52	2.26	5.34	4.43								3,013E-	1,019E-	5,068E-				

																				01	01	01	
pk135B	2.07	4.78	2.68	4.52	4.13	5.53	7.66	7.66	3.31	4.18	2.1	3.76	2.85	3.5	6.82	7.03				**9,591E-02**	4,684E-01	8,679E-01	
pk36A	97.32	35.21	112.33	26.4	93.85	41.13	70.39	30.18	127.23	28.42	116.45	30.56	77.87	25.99	73.4	39.38				**6,259E-02**	**5,169E-02**	1,310E-01	
pk122B	2	3	4.35	2.42	0.55	1.42	1.52	1.09	4.95	2.61	3.8	3.23	0.41	1.1	1.22	1.05				**2,916E-02**	8,493E-01	4,684E-01	
pk137B	3.34	5.58	8.01	6.95	18.07	27.81	40.14	38.89	5.82	4.31	7.43	4.99	8.7	10.27	26.7	27.13				**5,467E-02**	**6,660E-02**	6,163E-01	
pk44A	34.65	20.03	52.17	51.14	13.91	21.52	33.19	20.6	51.02	54.42	66.34	48.62	19.08	16.18	35.59	25.51				**4,154E-02**	**7,232E-02**	3,013E-01	
pk113	16.7	5.96	15.6	10.31	8.83	9.23	5.66	3.28	13.97	6.53	16.2	7.9	3.92	3.05	3.26	3.66				1,684E-01	**1,967E-05**	3,684E-01	
pk94B	2.45	3.73	1.98	4.11	2.46	1.14	1.71	0.84	2.82	3.23	3.41	3.22	1.39	1.68	0.94	1.35				1,740E-01	**3,210E-03**	5,540E-01	
pk35B	46.17	15.02	39.87	19.75	34.12	15.33	29.63	10.73	48.98	12.59	45.97	16.59	9.31	6.82	8.39	5.94				5,540E-01	**1,158E-11**	6,163E-01	
pk80B	13.64	7.2	23.93	13.22	5.13	4.47	3.15	1.57	34	12.62	39.14	15.63	4.47	3.58	4.76	4.73				**8,245E-02**	2,817E-01	**6,449E-02**	
pk126A	55.96	13.37	61	14.63	31.99	9.58	29.9	8.93	74.33	13.35	72.87	14.58	30.76	8.85	27.4	10.35				4,365E-01	7,462E-01	8,443E-01	
pk87B	4.23	4.93	11.26	5.64	0.28	9.75	1.83	1.27	8.88	4.68	8.3	6.75	1.6	3.58	2.16	3.07				1,710E-01	**5,289E-02**	2,142E-01	
pk109A	91.58	32.1	99.61	28.37	65.43	22.79	54.86	20.6	126.49	20.38	126.5	23.35	57.22	17.14	56.09	21.84				**8,461E-02**	1,710E-01	**9,551E-02**	
pk95B	7.67	2.87	9.21	6.1	0.9	4.75	3.61	2.63	5.77	4.34	6.96	5.08	2.5	2.45	4.34	5.23				**1,482E-02**	**5,196E-03**	**7,745E-02**	
pk211	1.74	3.96	2.14	1.61	1.56	2.81	0.55	0.47	2.62	2.48	2.64	2.31	0.36	0.73	0.27	0.64				1,876E-01	**1,866E-03**	3,013E-01	
pk48B	4.62	8.83	12	16.7	2.44	3.72	3.63	6.18	3.94	5.26	3.91	10.2	1.97	5.09	7.85	11.07				7,384E-01	4,684E-01	1,349E-01	

940

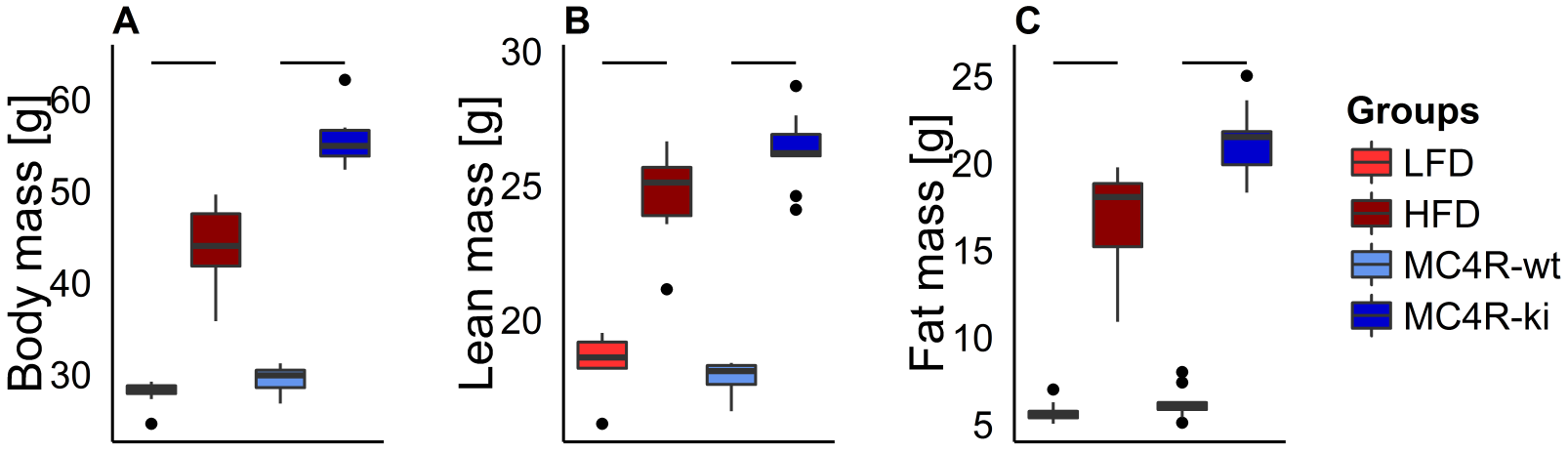
A
Body mass [g]
60
50
40
30
B
Lean mass [g]
30
25
20
C
Fat mass [g]
25
20
15
10
5
Groups
LFD
HFD
MC4R-wt
MC4R-ki

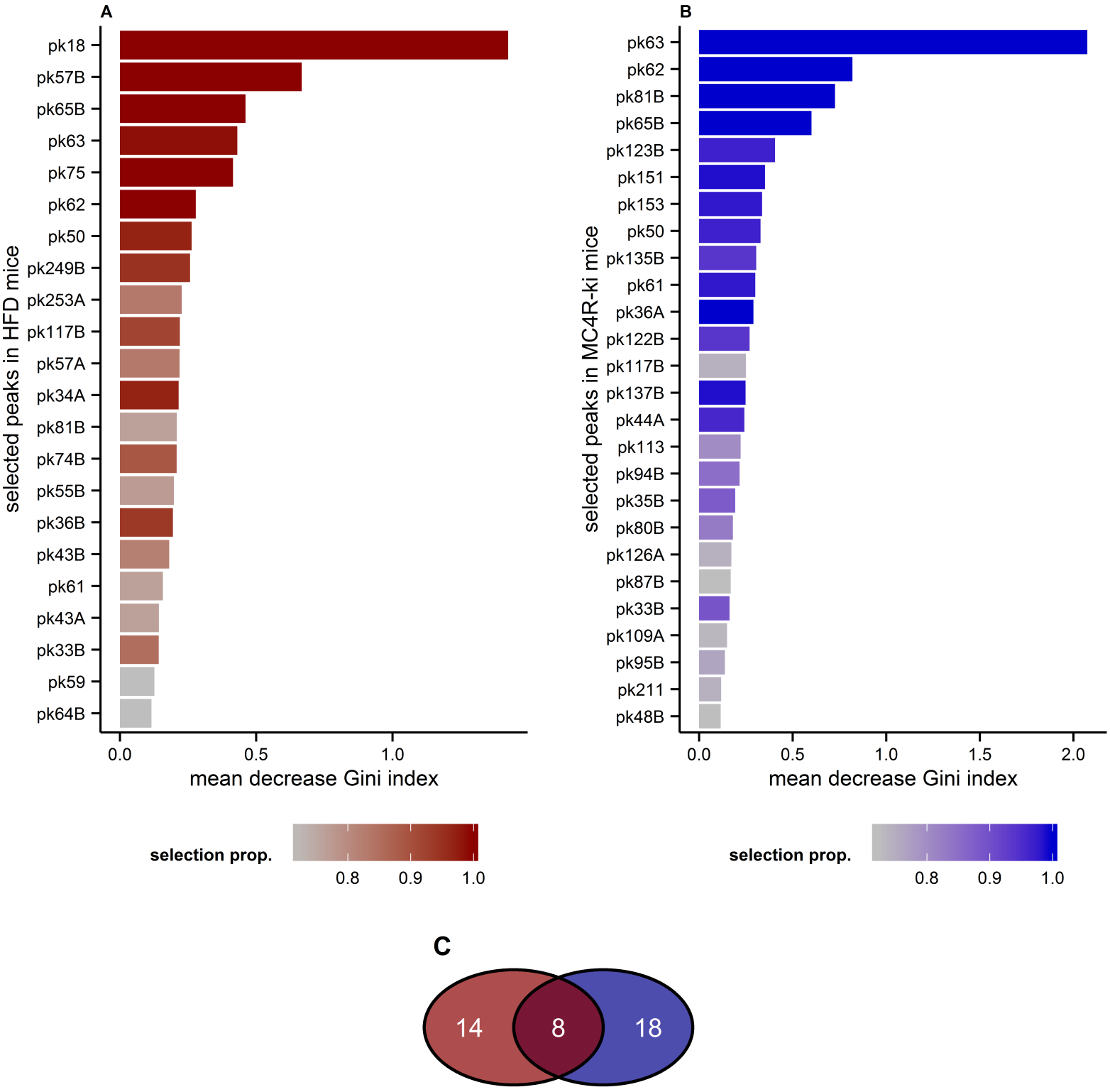
A
pk18
pk57B
pk65B
pk63
pk75
pk62
pk50
pk249B
pk253A
pk117B
pk57A
pk34A
pk81B
pk74B
pk55B
pk36B
pk43B
pk61
pk43A
pk33B
pk59
pk64B
selected peaks in HFD mice
0.0
0.5
1.0
mean decrease Gini index
selection prop.
0.8
0.9
1.0
B
pk63
pk62
pk81B
pk65B
pk123B
pk151
pk153
pk50
pk135B
pk61
pk36A
pk122B
pk117B
pk137B
pk44A
pk113
pk94B
pk35B
pk80B
pk126A
pk87B
pk33B
pk109A
pk95B
pk211
pk48B
selected peaks in MC4R-ki mice
0.0
0.5
1.0
1.5
2.0
mean decrease Gini index
selection prop.
0.8
0.9
1.0
C
14
8
18

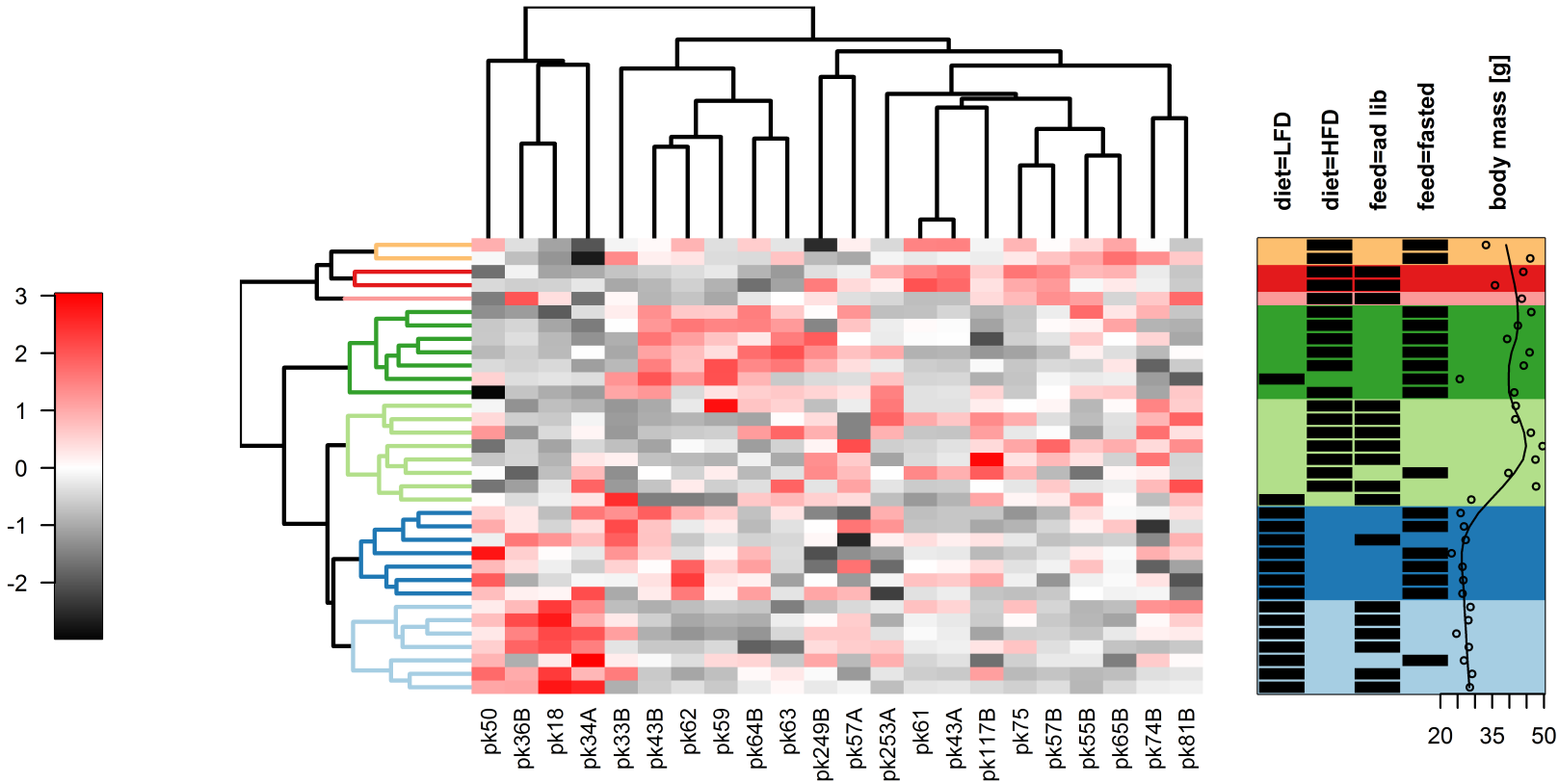
3
2
1
0
-1
-2
pk50
pk36B
pk18
pk34A
pk33B
pk43B
pk62
pk59
pk64B
pk63
pk249B
pk57A
pk253A
pk61
pk43A
pk117B
pk75
pk57B
pk55B
pk65B
pk74B
pk81B
diet=LFD
diet=HFD
feed=ad lib
feed=fasted
body mass [g]
20
35
50

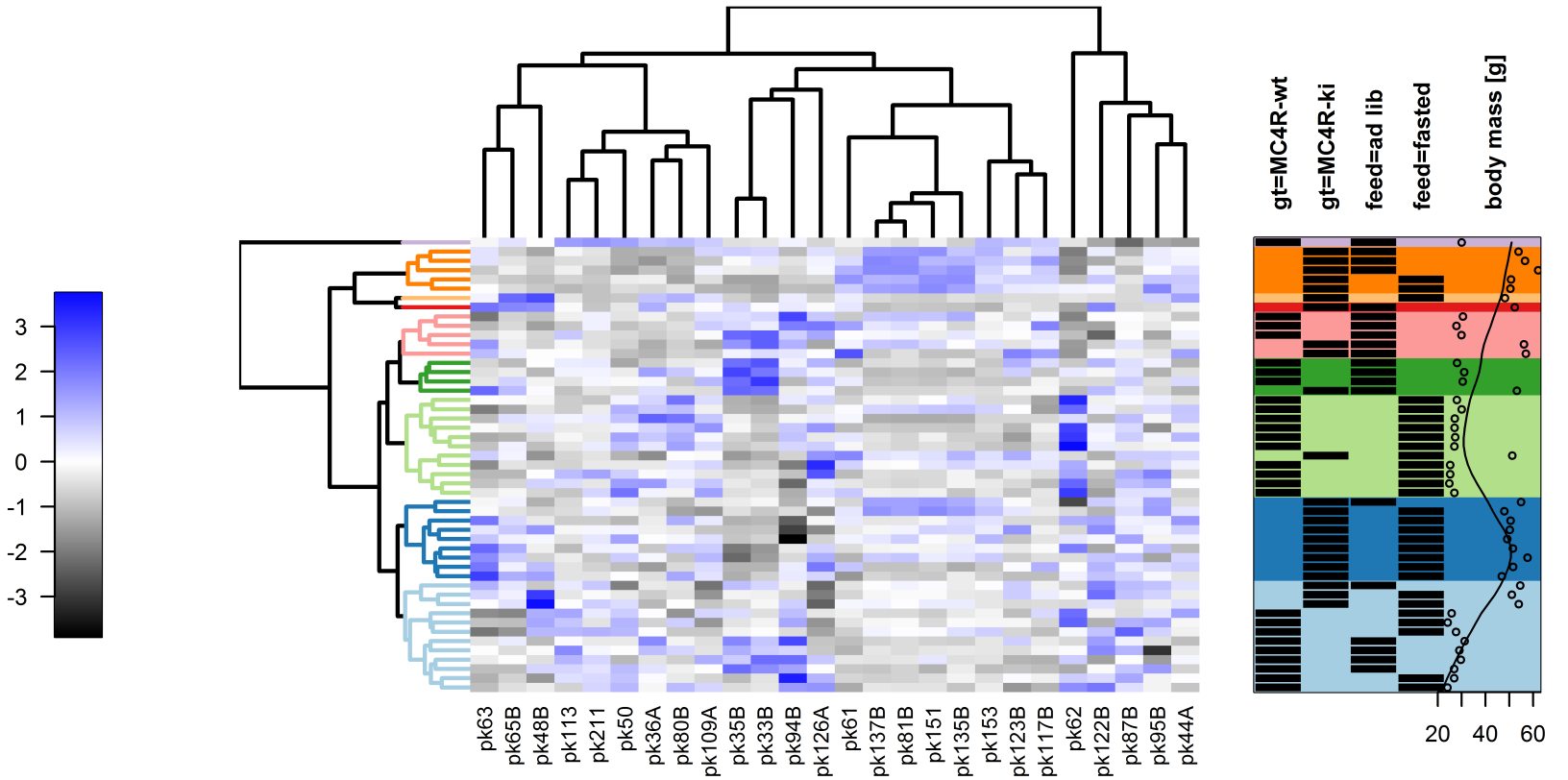
3
2
1
0
-1
-2
-3
pk63
pk65B
pk48B
pk113
pk211
pk50
pk36A
pk80B
pk109A
pk35B
pk33B
pk94B
pk126A
pk61
pk137B
pk81B
pk151
pk135B
pk153
pk123B
pk117B
pk62
pk122B
pk87B
pk95B
pk44A
gt=MC4R-wt
gt=MC4R-ki
feed=ad lib
feed=fasted
body mass [g]
20
40
60

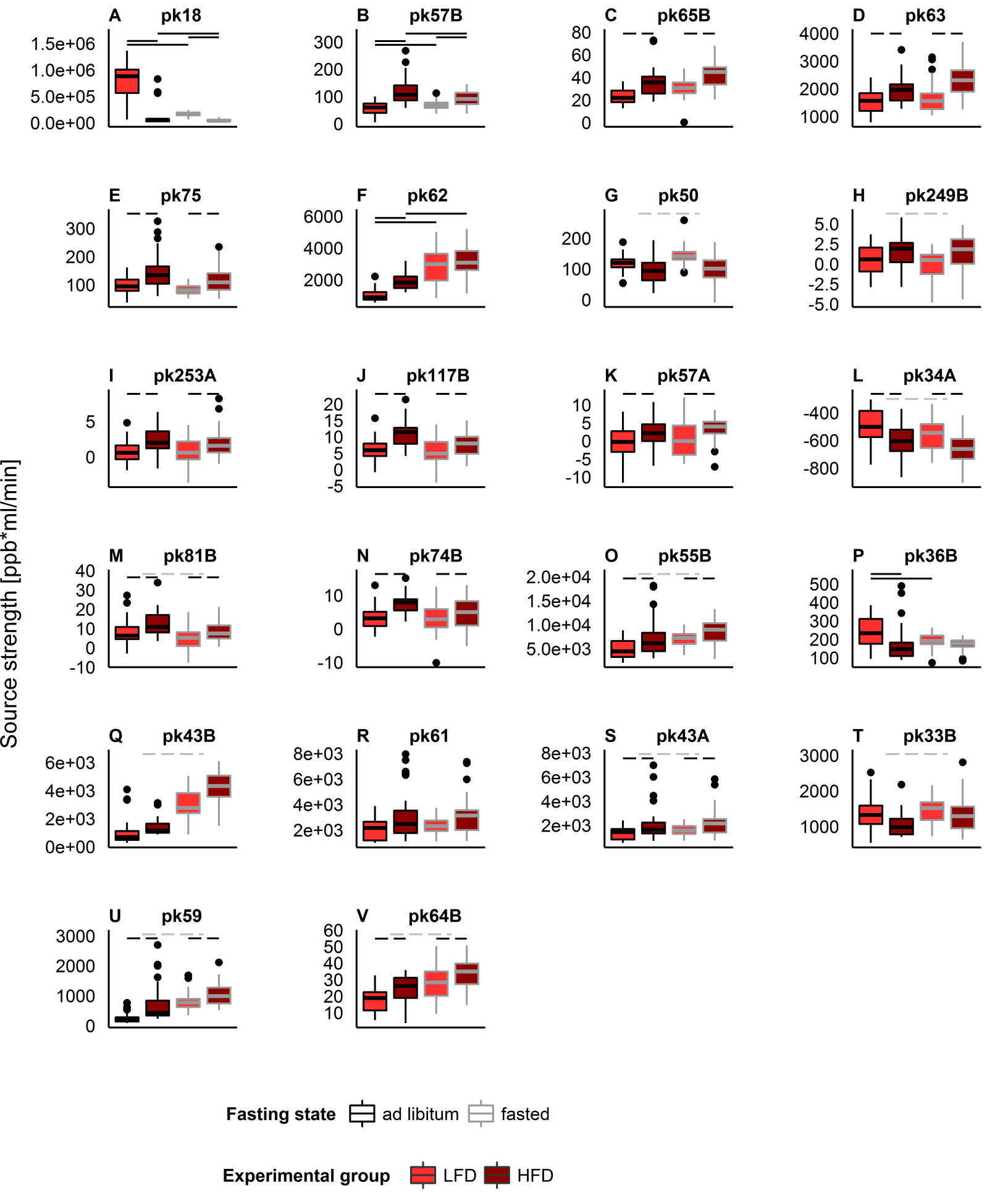
A pk18
B pk57B
C pk65B
D pk63
E pk75
F pk62
G pk50
H pk249B
I pk253A
J pk117B
K pk57A
L pk34A
M pk81B
N pk74B
O pk55B
P pk36B
Q pk43B
R pk61
S pk43A
T pk33B
U pk59
V pk64B
Source strength [ppb*ml/min]
Fasting state
ad libitum
fasted
Experimental group
LFD
HFD

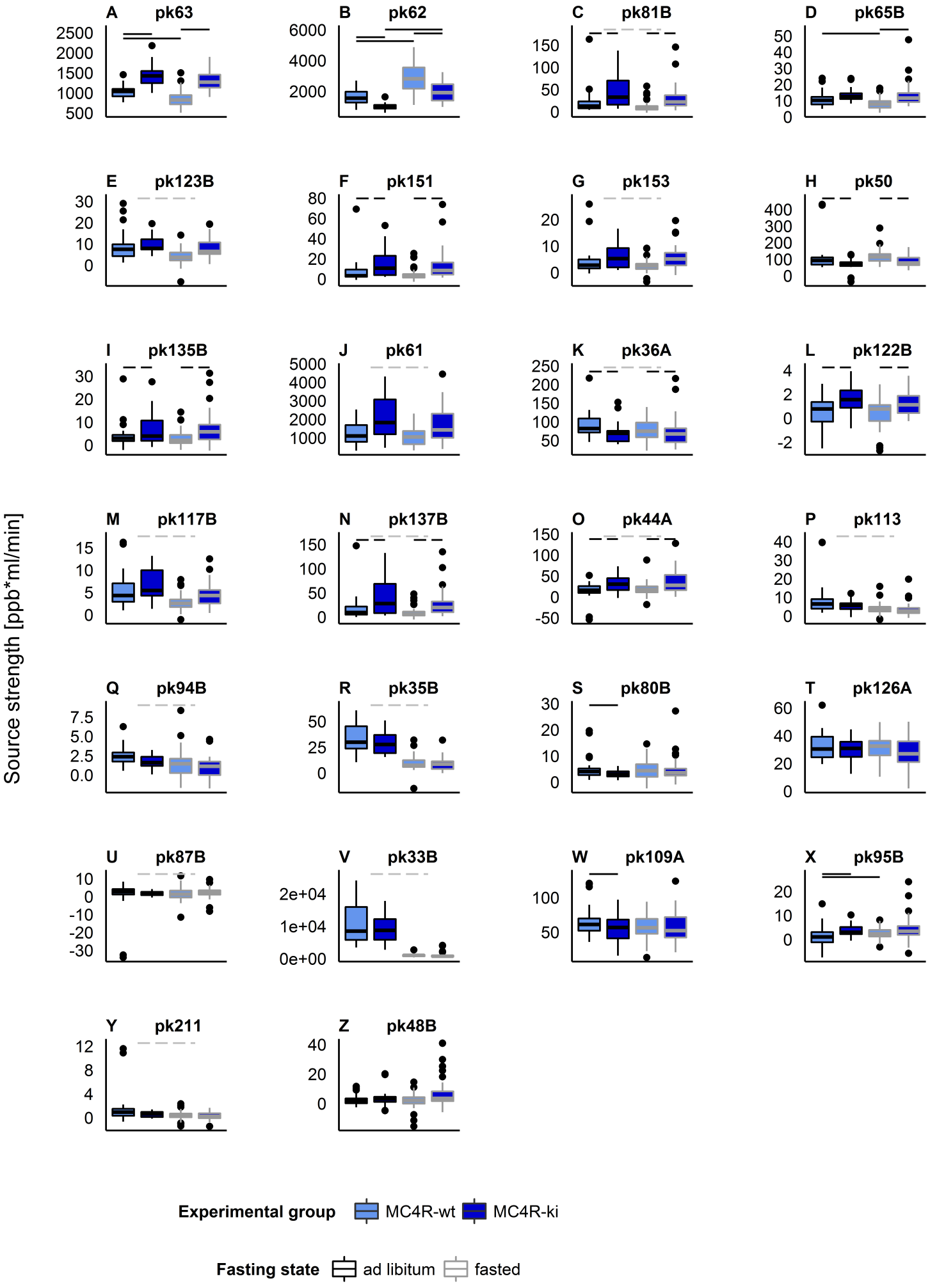
A pk63
B pk62
C pk81B
D pk65B
E pk123B
F pk151
G pk153
H pk50
I pk135B
J pk61
K pk36A
L pk122B
M pk117B
N pk137B
O pk44A
P pk113
Q pk94B
R pk35B
S pk80B
T pk126A
U pk87B
V pk33B
W pk109A
X pk95B
Y pk211
Z pk48B
Source strength [ppb*ml/min]
Experimental group MC4R-wt MC4R-ki
Fasting state ad libitum fasted

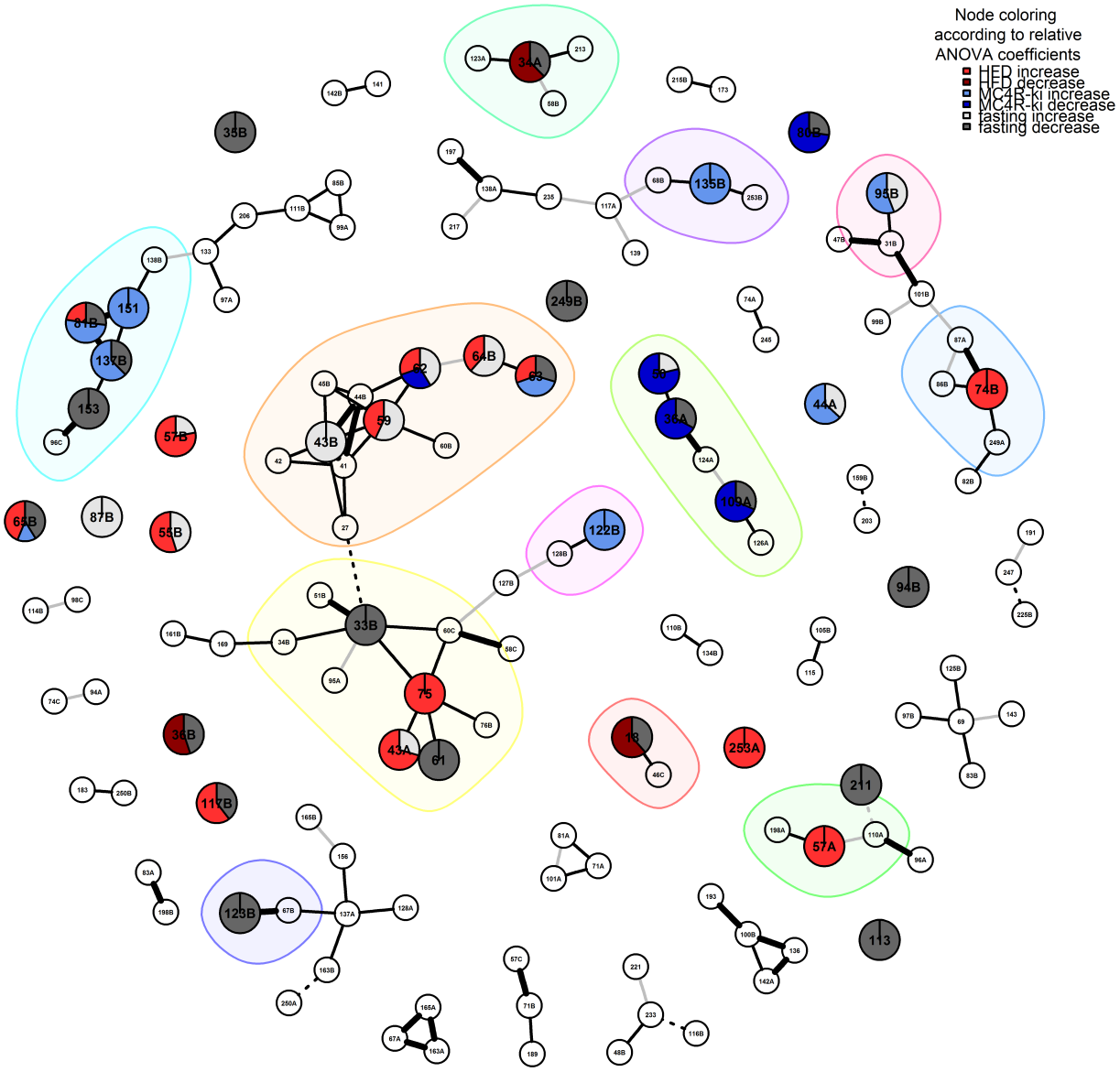
Node coloring
according to relative
ANOVA coefficients
HFD increase
HFD decrease
MC4R-ki increase
MC4R-ki decrease
fasting increase
fasting decrease